Int. J. Production Economics 284 (2025) 109567

Contents lists available at ScienceDirect

International Journal of Production Economics

journal homepage: www.elsevier.com/locate/ijpe

The diverging control policy's hand in supranational supply chain reconfiguration

Jan B. Broekaert *, Davide La Torre, Faizal Hafiz, Xavier Brusset

SKEMA Business School, Université Côte d'Azur, Sophia Antipolis, France

ARTICLE INFO

Keywords:
Supply chain performance
Mitigation policy
Network epidemics
Nash equilibrium

ABSTRACT

The efficiency of supranational supply chains is frequently compromised by divergent and evolving policies across countries. A novel assessment method for prolonged disruptive circumstances is presented, wherein supply chain performance is influenced by various mitigating control policies. The impact of control policies with concomitant labor productivity losses and perturbed delivery capabilities in supply chain networks is demonstrated through a detailed epidemic case study with diverging control approaches. First, a game-theoretic framework is employed through which the cost-optimal Nash equilibrium profile of diverging control strategies between countries is determined. Subsequently, cost-based strategic options for supply chain relocation are revealed through numerical simulations, providing guidance for entrepreneurial decision-making. The analysis is conducted on a realistically designed multiplex network that integrates a supply chain network layer with the case study's epidemic SEIRD-diffusion layer. Two interconnected countries with distinct GDPs are examined as they implement Nash equilibrium policies for Epidemic Control Cost (ECC). These policies are characterized by *strong* versus *weak* confinement, and *higher* versus *lower* vaccine efficiency. Through this innovative methodology, an explanation of policymakers' diverging mitigation policies and the potential decisions for supply chain relocation toward the comparatively better-protected region are elucidated, with consideration given to each region's Cost from Relocation and supply chain capacity Loss (LRC).

1. Introduction and context

A major case of international disparity unfolding in policy regulation transpired during the epidemic episode caused by COVID-19. The impact of the epidemic elicited effectively different policies from governments and health authorities worldwide with pervasive regional economic consequences at the macroeconomic level (Jackson et al., 2021; Ajmal et al., 2021) as well as microeconomic level (Lofvers, 2020). The manufacturing, processing, and shipping actors along supply chains saw their ability to produce at expected capacity unpredictably curtailed causing inventory problems, stockouts, commodity price hikes, and customer dissatisfaction (Lofvers, 2020; Hille, 2021; Ardolino et al., 2022). Public policymakers have deployed mitigating health strategies based on the modeling of epidemic dynamics (Bertozzi et al., 2020; Godio et al., 2020; Reicher and Stott, 2020; Boucekkine et al., 2021; MacIntyre et al., 2021; Xu et al., 2021; Yang, 2021; Amir and Boucekkine, 2022; Dobson et al., 2023). Such different sanitary strategies, through various implementations of social distancing to reduce transmission and vaccination policies to augment immunity, aim to minimize the epidemic *burden* or quantifiable impact in economic and human-life terms in their respective jurisdictions, but inherently inflict collateral damage to the common functioning of the economic process.

The combined effect of *concurrent* mitigating strategies from different international policymakers on likewise widespread supply networks has remained under-researched. The purpose of our work is to predict how supply chain capability to produce at nominal capacity is impacted by mitigating strategies put in place by aligned or non-aligned policymakers. We aim to provide model-based insights for managerial decision-makers as well as policymakers by providing a game-theory-based method that can be applied to configurations with regulatory differences in general.

Our results show how supply networks will be redrawn under prolonged epidemic circumstances and persistent national epidemic control policies. In particular, our work shows how unfolding divergent

* Corresponding author.
E-mail addresses: jan.broekaert@skema.edu (J.B. Broekaert), davide.latorre@skema.edu (D. La Torre), faizal.hafiz@skema.edu (F. Hafiz), xavier.brusset@skema.edu (X. Brusset).

https://doi.org/10.1016/j.ijpe.2025.109567
Received 20 August 2024; Received in revised form 11 February 2025; Accepted 20 February 2025
Available online 5 March 2025
0925-5273/© 2025 The Authors. Published by Elsevier B.V. This is an open access article under the CC BY license (http://creativecommons.org/licenses/by/4.0/).

policies drive the reconfiguration of supranational supply networks. Our original contribution lies at the intersection of public mitigation policy, network epidemics, and supply chain management to provide entrepreneurs, managers, and policymakers with an indicative framework of how public policies induce supply chain reconfiguration and affect the ability to serve final customers. Our method is based on deriving the *comparative encompassing control cost matrix* for the divergent mitigation policies of two international policymakers, to identify the optimal Nash-based strategy profile, and in consequence to assess the potential movement of supply chains. Our present work is hence a complementary study to Broekaert et al. (2024a), in which supply chain *resilience* and *viability* were forecast under various epidemic control scenarios. In our current study, the cost of possible supply chain reconfiguration –from throughput loss and relocation cost– is forecast and balanced with cost-based Nash profile health policies.

The remainder of the paper is organized as follows. As a pertinent case for divergent policies, Section 2 provides the significant literature references on studies that cover the behavior of supply chains under the influence of epidemics, the ensuing control politics, and on epidemiological models on social-contact networks. While the formalism of the epidemic network with diverging control strategies has been reported in detail previously in our study Broekaert et al. (2024c), a summary exposition is then given of the 'SEIRSD' model — named so for its defining population characteristics related to the stages of the disease; Susceptible, Exposed, Infectious, Recovered and Dead, and with a returning 'S' for waning immunity. Our innovative focus in our study is now the assessment of international supply chain performance, fully developed in Section 3. There, we cover the multiplex model with the epidemiological layer informing the **e**pidemic **c**ontrol **c**ost (ECC) of the public control policies for policy-makers and extend the graph with a production layer to model supply chain throughput **L**oss and its **R**elocation **C**ost (LRC) for managerial decision-makers. The simulations in Section 4 provide the numerical outcomes for the epidemic control policies and their corresponding perturbations for the supply chain throughput. These numerical results, for different macro-economic parametrizations, provide insight into the optimal management of supply chains depending on their embedding and the prevailing control strategic Nash equilibrium, discussed in Section 5. In the final Section 6, we conclude by highlighting our major insights into the assessment method for supply chain throughput under diverging mitigation policies.

2. Literature review; networks, supply chain performance and epidemics

Network models allow the detailed description of the dynamic interaction of realistic and diverse agents; ranging from individual persons to firms, cities or countries, describing the movement of goods and wealth, people and labor, or health and disease (Keeling and Eames, 2005; Newman, 2018). The effect of the **structure** of a contact network on the evolution of *epidemics* has been studied by Youssef and Scoglio (2011), Darabi Sahneh et al. (2013), Li et al. (2014), Sélley et al. (2015), Yang et al. (2017) and continued by, among others, Fagiolo (2020), Ottaviano and Bonaccorsi (2021), Großmann et al. (2021), Grabisch et al. (2022), Broekaert et al. (2022) and Rezapour et al. (2023) in COVID-19 settings. Some recent studies in disease epidemics have shifted the focus toward an **individual-based** ontology and toward the architecture of the contact network, e.g. Das et al. (2023)ad Dolgui et al. (2023). Our approach introduces **heterogeneity** at the individual level which renders a more realistic variation of outcomes from the disease and the epidemic control. This inclusion of detailed heterogeneity not only allows a more precise implementation of e.g. mitigating factors, but it also enables a procedure to assess the epidemic impact on labor productivity and supply chains. In a **multiplex** network approach additional features can be included, e.g. Fan et al. (2022b) encompass an *information layer* for disease awareness diffusion, and Peng et al. (2021) include a *competing opinions* layer over the social-contact network. In our current study, a productivity layer will inform the implicit throughput loss in supply chain networks. Epidemic models have been extensively developed to assess the mitigating effect of **control policies.** In the recent work of Eryarsoy et al. (2023) a compartmental SEIRD-model is heuristically solved in which government containment policies with weekly updates are implemented. Chen et al. (2023) build a SIRD-model with optimal health cost and SP500-based financial market stability. The modeling of the overall epidemic **cost** by Charpentier et al. (2020), Reddy et al. (2021), Gros et al. (2021), Gollier (2021), and Plazas et al. (2021), inform the policy cost-expression of the ECC in our approach in Section 3.2. A region's ability to deploy a specific mitigation plan is primarily related to its **GDP** and economic health. In the work of Aum et al. (2021), such a model is presented for the evolution of the GDP to monitor the deviation of the purported trade-off with public health (see Hevia et al. (2022)). In our model, Section 3.2, the GDP-difference of interdependent countries is shown to substantially affect the choice of the control policies based on their respective ECCs.

Game-theoretic interaction. The global contact network's interconnectedness means *local* control policies affect *distant* epidemic outcomes. During COVID-19, competition and collaboration emerged over scarce medical supplies (Farahani et al., 2023). While regulatory flexibility and political support proved crucial, competitive medical supply acquisition has been analyzed through game theory (Salarpour and Nagurney, 2021). The optimal solution emerges as a generalized Nash equilibrium due to *interdependent* regional outcomes (Nagurney et al., 2016; Nagurney, 2021a,b). In our model, the cost-effectiveness of local epidemic control strategies is influenced by foreign control measures. The interdependence of outcomes stems from epidemic diffusion between interconnected populations. Therefore, optimal outcomes for *competing* populations follow game-theoretic principles.

Supply chain disruptions. COVID-19's impact on supply chains and associated disruption management have been extensively studied and reported (Paul et al., 2021; Ouardighi et al., 2022). In particular, the *ripple effect* in the economic networks caused by lockdowns has been analyzed through various models (Borgatti and Halgin, 2011; Mishra et al., 2019; Kinra et al., 2020; Li and Zobel, 2020; Park et al., 2021; Llaguno et al., 2021; Ivanov et al., 2020; Ivanov, 2020; Yu and Aviso, 2020; Choi, 2021; Sawik, 2022; Scarpin et al., 2022; Brusset et al., 2022, 2023). Mitigation strategies include policies for pre-positioning and production-ordering, and *leagility* from intertwined networks (Rozhkov et al., 2022; Nikolopoulos et al., 2021; Dolgui et al., 2020). Network resilience is shown to enhance through supplier substitutability (Hosseini and Ivanov, 2019; Zahiri et al., 2018; El Baz and Ruel, 2021; Ivanov, 2021; Brusset et al., 2023; Ivanov et al., 2023). Recent advances include collaborative distribution optimization (Alikhani et al., 2023), resource management under epidemic migration (Jiang et al., 2024), intelligent digital twins for resilience analysis (Ivanov, 2023), immune system-inspired resilience frameworks (Ivanov, 2024), and adaptive operational decisions (Rozhkov et al., 2022). Quality propagation in hub-and-spoke networks has also been examined (Nuss et al., 2016; Berger et al., 2023). However, existing literature lacks models for supply network changes under macroeconomic health policy divergences and related tools for forecasting dynamics in an encompassing epidemic-and-production multiplex network, which Section 3 will address.

3. Supply chain throughput loss and relocation costs under epidemic control

Before detailing the supply chain optimization method under diverging control policies, a brief overview of the approach is provided. For a comprehensive understanding, the main principles of network diffusion and control are summarized, with formal details available in related studies (Broekaert et al., 2022, 2024c). This foundational model

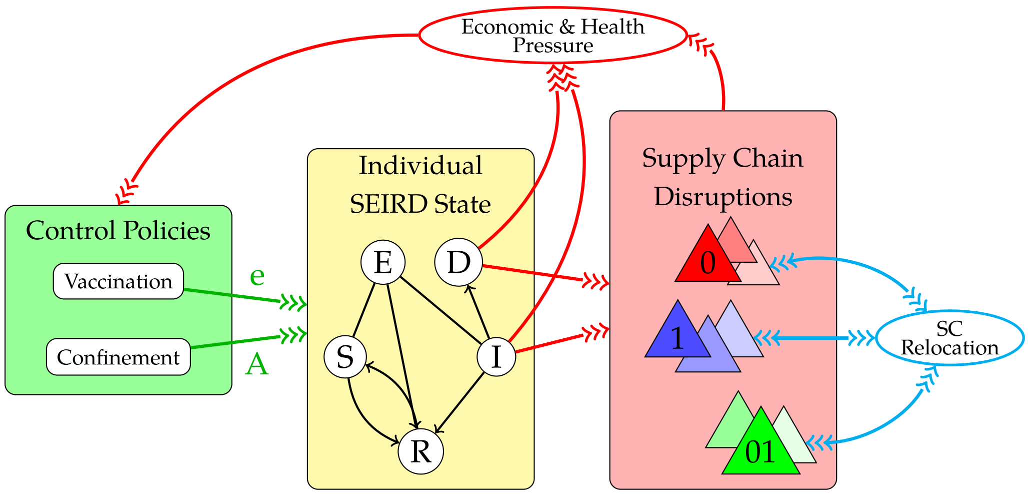

Fig. 1. The basic submodel interactions of Control Policies on Epidemic SEIRD-state evolution in all individuals, and the resulting Supply Chain Disruptions. The control policies impact the dynamics of the disease evolution. Typically, vaccination will diminish the Exposed to Infected flow, while Confinement reduces the Susceptible to Exposed flow. The throughput of Supply Chains in regions 0, 1, and supranational 01, economic strain, and population health will relate to Infected and Death amplitudes in the population. In response, long-term process optimization includes Supply Chain relocation.

develops the cost of control policies and leads up to the description of the cost of re-designing supply chains in response to divergent control policies. The model comprises two complementary sub-models.

The **first** is an epidemic-and-control model incorporating probabilistic SEIRD dynamics, a realistic heterogeneous contact network structure for epidemic diffusion, and a heterogeneous parametrization of the COVID-19 epidemic, Fig. 1. Basically, this epidemiological model tracks disease transmission events between individuals: when an infected individual interacts with a susceptible individual there exists a possibility that the later becomes infected. Within the SEIRD framework, each individual traverses through distinct disease states: Susceptible (S), Exposed (E), Infectious (I), Recovered (R), or Deceased (D). Fig. 1 illustrates the state transitions within an individual; for instance, the transition from state 'S' to 'E' is mediated by the contact matrix A, which aggregates all person–person contacts and hence disease exposure from neighboring infected individuals. Confinement control measures aim to modulate this 'adjacency' matrix A. While reducing the components in A diminishes disease transmission, it simultaneously constrains regular societal and economic functions. Public health intervention by vaccination programs, characterized by efficiency parameter e, aims for an individual's state transition toward Recovery ('R'). The precise monitoring of individual health states, with particular emphasis on improving workforce availability through increasing Recovered ('R') and Susceptible ('S') states, follows from the detailed disease dynamics as further illustrated in Fig. 2. The precise flows between an individual's potential stages of the disease over time are governed by the differential equations Eqs. (4) in Section 3.1, with each term's derivation briefly explained therein.

The SEIRD model, operating on the contact network, facilitates the computation of epidemic control costs at the national level. Inter-country divergences in control strategies and health policies reflect cultural, political, and economic factors. Their GDP difference serves as a proxy metric for cost differences in implementing measures like testing, contact tracing, expanding emergency healthcare, confinement and vaccination programs.

The **second** component is the formalism for comparing supply chain capacity loss and relocation costs (LRC) under diverging control policies. By adopting the health metric from the contact layer, the effective labor capacity of individuals in any 'economic production' conglomerate can be assessed. This metric is assumed to be proportional to the nominal supply chain's production, transport, and delivery capacity. Basically, a supply chain will be considered as a set of nodes that can be widely spread over the network and different countries. In the 'economic production' layer the edges between nodes now indicate membership to the same supply chain conglomerate. Since each individual node has a different labor capacity, some subsets will have higher economic throughput capacity than other sets that are highly impacted by the epidemic. In general, the throughput capacity of a supply chain will be best protected when health policies are effective and do not impede their functioning.

Our study aims to offer optimized management opportunities based on the compounded cost of supply chain throughput loss and the Restructuring-Relocation Cost (LRC), all under a joint control policy. This policy landscape is strategically derived from the optimized compounded cost of epidemic health policy, control strategy, and economic production loss, revealing the effect of the control policy context on supply chain decisions. This encompassing cost, ECC, will be formally expressed in Section 3.2,

3.1. Epidemics and the policymaker's mitigation model

In our model, two interconnected countries – represented as subpopulations of one encompassing supranational contact network – deploy possibly diverging control strategies imposed by their respective policymakers. Our current framework considers two contact-restraining confinement strategies: '*strict isolation & short duration*' (Css) versus '*weak isolation & long duration*' (Cwl). Also, two vaccination strategies are available; '*early deployment & lower-efficiency vaccination*' (Vel) versus '*later deployment & higher-efficiency vaccination*' (Vlh). Any possible combination of both the confinement and vaccination strategies or none can be selected. For clarity of the argument the health policies have been restricted to these nine specific control strategies

$$CS = [\mathrm{No}, \mathrm{Css}, \mathrm{Cwl}, \mathrm{Vel}, \mathrm{Vlh}, \mathrm{CssVel}, \mathrm{CssVlh}, \mathrm{CwlVel}, \mathrm{CwlVlh}], \tag{1}$$

for which the parametrizations are detailed in Section 4. Note that for tractability this is a restricted policy range, but qualitatively consistent with what we can observe in national authority choices in the world. For instance, the PR China has chosen a *strict isolation & short duration* with *early deployment & lower-efficiency vaccination*, whereas most West-European countries have chosen *weak isolation & long duration* with *later deployment & higher efficiency vaccination* (Yuan, 2022). A decisive factor in the severity of an epidemic is the density and length of paths along which the infection can be passed on throughout the population. In an individual-based contact network, $\mathcal{G}(V_{\mathcal{G}}, E_{\mathcal{G}})$, each node, from the vertex set $V_{\mathcal{G}}$, represents an individual, and each edge, from the set $E_{\mathcal{G}}$, between two nodes, stands for a contact with possible infectious

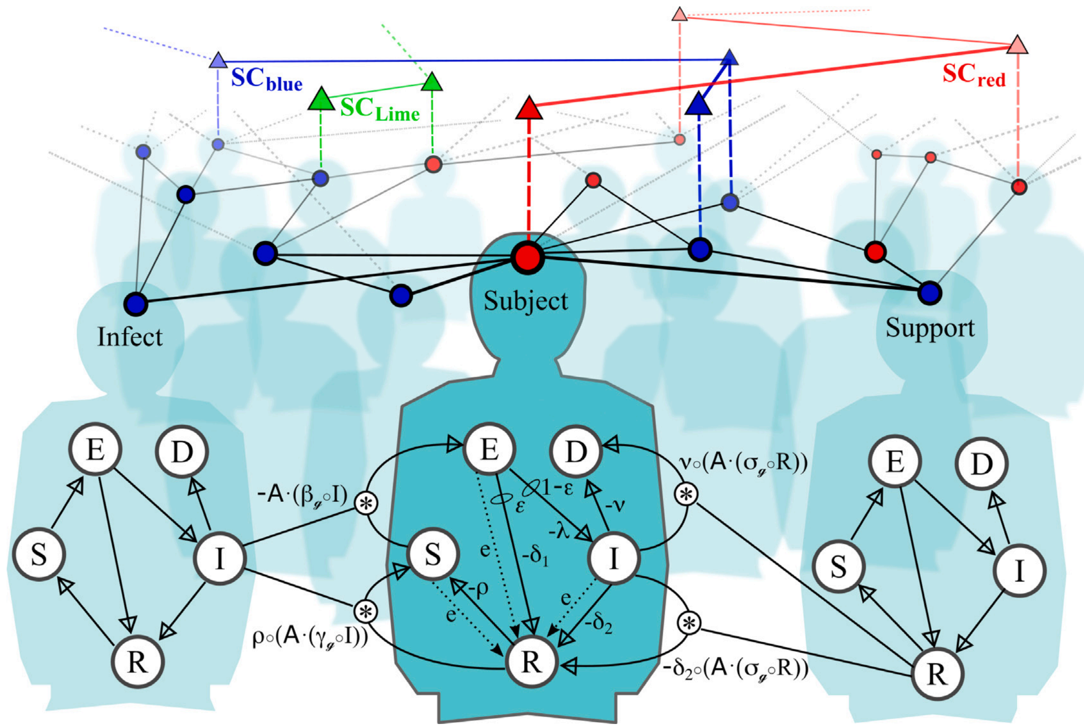

Fig. 2. The schematic multiplex network of supply chains and social contacts. Top layer: a supply chain composed in country-0 (red triangles), country-1 (blue triangles), and with supranational composition (lime triangles). Middle layer: the social contact network over the nodes of two populations (blue circles and red circles). Bottom silhouettes: SEIRSD dynamics and vaccination process with three possible roles of each individual. Flow from Susceptible to Exposed (infection rate $\beta_{\mathscr{G}}$), then to Infectious (latency λ) or Recovered (first recovery δ_1). The common $E \rightarrow I$ flow is weighted dominantly ($1 - \epsilon$), in comparison to the rare $E \rightarrow R$ flow (ϵ). The flow splits from Infectious to Recovered (second recovery δ_2) or Dead (virality ν). The waning immunity leads Recovered back to Susceptible (immunity waning ρ). Due to vaccination (efficiency e), the Recovery in-flows increase. The ego-network effects of the "infection role" ($\beta_{\mathscr{G}}$ and re-exposure $\gamma_{\mathscr{G}}$), and "support role" ($\sigma_{\mathscr{G}}$) increase (-) or diminish (+) the amplitude of the flows.

transmission (e.g., in a day). From the perspective of a single node, all the immediate neighbor nodes form the *ego-network* and constitute the source of possible infection for this individual. In practice, each individual in the encompassing network – with their personal characteristics – has a probability of becoming ill depending on the compounded effect of infectious contacts in their specific local ego-network. The epidemic diffusion is modeled on an individual-based network according to probabilistic SEIRSD-dynamics (see below) and allows the extraction of *SEIRD-load* metrics to monitor the epidemic magnitude for policy purposes (Broekaert and La Torre, 2021; Broekaert et al., 2022, 2024c). Our model considers five different compartment-based characteristics for each individual; Susceptible (S), Exposed (E), Infectious (I), Recovered (R), and dead (D), through which an individual evolves according to personal idiosyncrasies of age, comorbidity, or weakened immune system and waning immunity, see Fig. 2.

The SEIRD epidemic dynamic attributes to each five a probability that informs their state of being in one of the respective conditions $\{S, E, I, R, D\}$:

$$\boldsymbol{\Pi} k(t) = \left(p_{S,k}(t), p_{E,k}(t), p_{I,k}(t), p_{R,k}(t), p_{D,k}(t)\right). \tag{2}$$

These probabilities can be re-grouped into graph-based N-dimensional segment vectors

$$\mathbf{p}_X(t) = (p_{X,1}(t), \ldots, p_{X,N}, (t)) \tag{3}$$

defined for each of the characteristics $X \in \{S, E, I, R, D\}$ These probabilities will evolve depending on the disease's impact on each node's ego-network. This local network is variable for each individual since it includes only those edges of the full graph $E_{\mathscr{G}}$ for which the individual is the central node and connected to its first neighbors. The *adjacency* of nodes, mapped by the matrix A, is, therefore, a decisive factor in the progression of an epidemic. In practice, the individual-based model generalizes the original approach (Kermack and McKendrick, 1927), in which the infectious force is set proportional to the product of receptive (S) and emitting (I) components. Similar product terms have been included for social effects of care (Wong and Kohler, 2020/09/25) and the effect of re-exposure in immunity loss (Wu et al., 2021), besides terms for the observed waning of immunity (Levin et al., 2021; Saad-Roy et al., 2020). The latter effect of waning immunity introduces the possibility of a cyclic trajectory since the Recovered component can decay back into the Susceptible component, hence the denotation 'SEIRSD' network model. This probabilistic approach extends the *N-intertwined mean-field approximation* of Pastor-Satorras et al. (2015), Prasse et al. (2021), and Darabi Sahneh et al. (2013). In more detail, the epidemic system includes the following factors for each node in its governing equations;

i. (S→E) The fundamental mechanism driving epidemic spread is the **exposure** of susceptible individuals to the pathogen through contact with infected individuals. When such contact occurs, the virus may be transmitted to the susceptible person, driving their flow from the susceptible to the exposed component. In practice, all infectious individuals in a person's direct contact network can be conducive to this exposure. Formally, the exposure process is captured by the infection term $\mathbf{F}_{IS;\beta} = \mathbf{p}_S \circ A(\boldsymbol{\beta}_{\mathscr{G}} \circ \mathbf{p}_I)$, which combines three factors: the individual's probability of being susceptible $\mathbf{p}_S$, their contact network structure A, and the infection potential $\boldsymbol{\beta}_{\mathscr{G}} \circ \mathbf{p}_I$ of infectious components from neighbor-node individuals. Each person simultaneously acts the roles of a potential 'susceptible subject' and potential 'infector' based on their SEIRD probabilities, as illustrated in Fig. 2. Note that the epidemic parameter values need to be calibrated according to the ego-network size and average network degree, following Broekaert et al. (2024c).

ii. (E→I and E→R) After **exposure**, individuals typically progress through an incubation period before potentially becoming infectious. Most exposed individuals will develop the disease and

Table 1
The (averages of) epidemic parameter values used in the simulation experiment on a designed contact graph. Initially, the N-sized population is randomly seeded with N_{init} infected individuals. The individual epidemic values are derived from the lognormal distribution of each parameter with standard deviation fixed at fraction SD_{frac} of its average value. A detailed discussion of the SEIRSD parametrization is given in Broekaert et al. (2024c).

β	δ_1	δ_2	λ_l	v	ρ	γ	σ	ε	SD_{frac}	N	N_{init}
.95	$\varepsilon \cdot 1/4$	1/6	$(1-\varepsilon) \cdot 1/4$	.001	1/180	.1	.1	.03	.05	1000	10
Comp. infect.	First recovery	Sec. recovery	Latency	Mortality	Immun. waning	Vir. re-exp.	Soc. strength	Chann. weight	Heterogeneity	Population size	Initial infected

become infectious themselves, while a small fraction may naturally clear the infection and flow directly to the Recovered component. The flow to the infectious component occurs at rate λ (latency parameter), expressed as $\mathbf{F}_{E;\lambda} = \lambda \circ \mathbf{p}_E$, and dominates with weight 1-ε. The less common direct recovery flow occurs at rate $\boldsymbol{\delta_1}$ (primary recovery parameter), given by $\mathbf{F}_{E;\delta_1} = \boldsymbol{\delta}_1 \circ \mathbf{p}_E$, with weight $\varepsilon \ll 1$ (Fan et al., 2022a).

iii. (I→R) Most individuals will **recover** from the disease and build up an immune response to the virus. Each of these individuals will recover over time according to their ('second') recovery rate parameter $\boldsymbol{\delta_2}$. This flow to the recovery state is expressed by $\mathbf{F}_{I;\delta_2} = \boldsymbol{\delta}_2 \circ \mathbf{p}_I$. The recovery process is enhanced when the social environment is not worn down by the epidemic. This factor from *healthy* social support, scaled by $\boldsymbol{\sigma}$, is obtained from an individual's ego-network's Recovered components $\mathbf{F}_{I,R;\delta_2,\sigma} = \boldsymbol{\delta}_2 \circ \mathbf{p}_I A \boldsymbol{\sigma}_{\mathcal{G}} \circ \mathbf{p}_R$. This social effect corresponds to each individual's potential role of 'supporter' in other's recovery process, Fig. 2.

iv. (I→D) A fraction of the infected individuals will **succumb** to the disease. These infected individuals will leave the dynamics by irreversible absorption in the death component. Depending on their constitution's vulnerabilities, their individual virulence rate $\boldsymbol{v}$ and the severity of their infection component, the virulence term $\mathbf{F}_{I;v} = \boldsymbol{v} \circ \mathbf{p}_I$ quantifies their mortality flow. Again, social support from an individual's ego-network's Recovered components can decrease that individual's mortality risk, Fig. 2, and hence diminish the flow to their death component, $\mathbf{F}_{I,R;v,\sigma} = \boldsymbol{v} \circ \mathbf{p}_I \circ A(\boldsymbol{\sigma}_{\mathcal{G}} \circ \mathbf{p}_R)$.

v. (R→S) Individuals who have recovered from the disease, and those who received appropriate vaccination enjoy immunity from the disease. In practice, this protection has been shown to be temporary (Saad-Roy et al., 2020; Levin et al., 2021). Each individual's immunity component will wane over time according to their immunity loss rate $\boldsymbol{\rho}$, and reduce the Recovered component according to $\mathbf{F}_{R;\rho} = \boldsymbol{\rho} \circ \mathbf{p}_R$. However, periodic re-exposure to the pathogen through contact with infectious individuals can boost immunity, reducing the rate of immunity loss (Wu et al., 2021). This immune-boosting effect from re-exposure to all infectious components in their ego-network *diminishes* their immunity waning according to $\mathbf{F}_{R,I;\rho,\gamma} = \boldsymbol{\rho} \circ \mathbf{p}_R \circ A(\boldsymbol{\gamma}_{\mathcal{G}} \circ \mathbf{p}_I)$.

These factors lead to the $5 \times N$ coupled governing equations of the graph-based epidemic system:

$$\frac{d}{dt}\begin{bmatrix} \mathbf{p}_S \\ \mathbf{p}_E \\ \mathbf{p}_I \\ \mathbf{p}_R \\ \mathbf{p}_D \end{bmatrix} = \begin{bmatrix} -\mathbf{F}_{IS;\beta} + \mathbf{F}_{R;\rho} - \mathbf{F}_{R,I;\rho,\gamma} \\ \mathbf{F}_{IS;\beta} - (1\text{-}\varepsilon)\mathbf{F}_{E;\lambda} - \varepsilon \mathbf{F}_{E;\delta_1} \\ (1\text{-}\varepsilon)\mathbf{F}_{E;\lambda} - \mathbf{F}_{I;\delta_2} - \mathbf{F}_{I,R;\delta_2,\sigma} - \mathbf{F}_{I;v} + \mathbf{F}_{I,R;v,\sigma} \\ \varepsilon \mathbf{F}_{E;\delta_1} + \mathbf{F}_{I;\delta_2} + \mathbf{F}_{I,R;\delta_2,\sigma} - \mathbf{F}_{R;\rho} + \mathbf{F}_{R,I;\rho,\gamma} \\ \mathbf{F}_{I;v} - \mathbf{F}_{I,R;v,\sigma} \end{bmatrix} \tag{4}$$

It is easily verified that this system conserves the total state probability for each node by noticing that all terms on the right-hand side cancel on summation; $|\boldsymbol{\Pi} k(t)|_1 = 1, \forall k \in [1 \cdots N], \forall t \in \mathbb{R}^+$. (The parameter values are reported in Table 1).

The vaccination process is implemented in the model by a *formal* recalibration of an individual node's state vector. The vaccination process – when successful – will render an individual immune to the disease, therefore amounting to amplifying the Recovered 'R' state. Hereto, the vaccination process transforms the treated nodes according to the weighting of the R-boosted state and its unaltered previous state

$$\Pi_k(t+dt) = e\,(1\text{-}e, 0, 0, e\text{-}p_{Dk}(t), p_{Dk}(t)) + (1\text{-}e)\,\Pi_k(t) \tag{5}$$

into the next time step. This implementation of the vaccination process conserves the L_1 norm of the individual's SEIRD state vector, Eq. (2), and warrants the probabilistic interpretation of its amplitudes. Note that when the vaccine efficiency $e = 0$, the state remains unaltered (not considering a placebo effect), while when the efficiency $e = 1$ a fully Recovered state is obtained (not considering a Lazarus effect). The vaccination policy will randomly sample and R-boost, Eq. (5), a country's individuals within a programmed window of time and to a pre-fixed fraction of the population.

In sum, the implemented SEIRD-evolution comprises the continuous infection dynamics, Eqs. (4), and the stochastic R-boosting state re-weighting from vaccination, Eq. (5).

SEIRD-loads. The control strategies and their specific parametrization depend on the longitudinal development of the magnitude of the *constrained* versus the *unconstrained* epidemic. We define the *load* metric based on the worst impact of the epidemic over the longitudinal time range T of the epidemic:

$$X_{load} = \frac{1}{N}\sum_{j \in V_{\mathcal{G}}} \max_t \left(p_{X_j}(t)\right), \quad t \in T, \forall X \in \{S, E, I, R, D\}. \tag{6}$$

Using our probabilistic approach of the SEIRSD-epidemic on a social-contact graph, Eq. (4), for each node, a probability of allocation to the five different compartment-based characteristics $\{S, E, I, R, D\}$ can be calculated for all time periods.

In particular, the effectiveness of the control scenarios will be quantified by their resulting EID-loads in the encompassing cost expression, Eq. (8), for ECC, in the next section. The observed and forecast SEIRD-loads, Eq. (6), in the population – typically the I-load, metric for worst infectious accumulation, and D-load, metric for worst death accumulation – will trigger epidemic containment efforts following a governmental policy. These in turn will affect the performance capacity of the supply chains, Section 3.3.

3.2. Epidemic control cost

First, we comment on the policymaker's cost of epidemic control policy, Eq. (8), or ECC. The deployed containment efforts will be assessed depending on the forecasted magnitude of the *unconstrained* and the *controlled* epidemic. In practice, the forecast SEIRD-loads in the population, described in Eq. (6), will trigger the governmental epidemic containment policy and inform the required severity of health measures. The probabilistic system state vectors $\mathbf{p}_R$ and $\mathbf{p}_S$, Eq. (4), provide the fraction of the network sub-population which maintains a productive role during the epidemic, and can be expressed complementarily through $\mathbf{p}_E$, $\mathbf{p}_I$, and $\mathbf{p}_D$. These dynamic system variables inform the SEIRD-loads which appear in the cost expressions.

Second, we outline the basic cost expression related to diminished supply chain throughput under a specifically *controlled* epidemic. Our

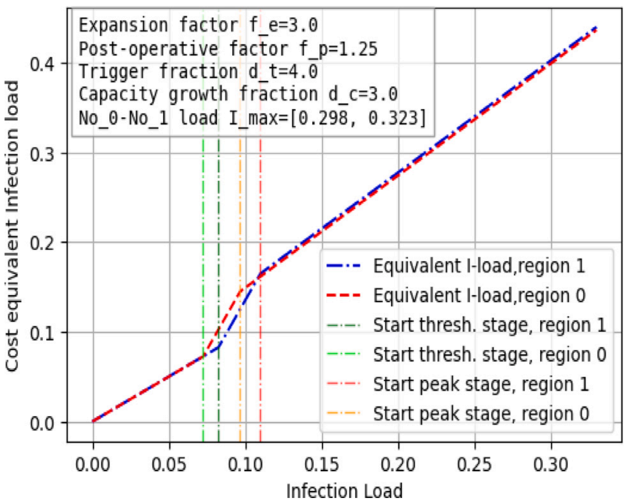

Fig. 3. The public health capacity limitation and response to epidemic outbreak $\mathcal{J}$, Eq. (7), is modeled with three stages depending on infectivity I_α: The trigger-fraction d_t w.r.t the worst case scenario for developing supplementary capacity. The capacity fraction d_c capping the expansion effort. The expansion factor f_e scales for the investment cost of the capacity expansion, and the post-operation factor f_p scales for the augmented equivalent cost in the peak stage of the epidemic after the capacity increase. .

model provides a method to inform managers and entrepreneurs of the optimal repositioning of their supply chain nodes based on projected *supply chain loss of throughput*, C_{cap}. Depending on the possible non-alignment between 'national' health priorities and regional supply chain performance loss, compounded with the cost of re-positioning supply chain nodes, C_{mig}, an *optimal choice* can be identified. In order to assess the epidemic's impact on supply chain throughput, a practical procedure is fixed for the supranational networks. Our model considers two embeddings of supply chains: national ('*country-0*' and '*country-1*') and supranational (labeled '01'). Under diverging control strategies, each embedding of a supply chain is impacted differently. To obtain consistently representative results, the averaged performance loss, cap_{SC0}, cap_{SC1} and cap_{SC01}, over a fixed number of randomly sampled supply chains will be defined (see Eqs. (16)).

The policymaker's ECC is subdivided into four components, as described in more detail in Broekaert et al. (2024c); (i) the control strategy cost which covers the aid in development, production, and dispensing of a vaccine, and the confinement logistics, (ii) the health policy cost for epidemic mitigation scaled to the number of infection cases $\mathcal{J}(I_\alpha, I_{max_\alpha})$. This cost reaches a threshold when the capacity of the health infrastructure is challenged and supplementary investments are required (Freiberger et al., 2022), and at a further increased infection stage, is assumed to increase due to adaptive operation

$$\mathcal{J}(I_\alpha, I_{max_\alpha}) = \begin{cases} I_\alpha \quad : I_\alpha < I_{max_\alpha} d_t^{-1} \\ I_{max_\alpha} d_t^{-1}\left(1 - f_e\right) + f_e I_\alpha \quad : I_{max_\alpha} d_t^{-1} < I_\alpha < I_{max_\alpha} d_c^{-1} \\ I_{max_\alpha}\left(d_t^{-1}(1-f_e) + d_c^{-1}(f_e - f_p)\right) + f_p I_\alpha \quad : I_\alpha > I_{max_\alpha} d_c^{-1} \end{cases} \tag{7}$$

where $I_{max_\alpha} = I_{\mathrm{No}_0\text{-}\mathrm{No}_1}$ for each country $\alpha \in \{0, 1\}$, Broekaert et al. (2024c) (see Fig. 3).

Further cost components cover, (iii) the value of lost human life and, (iv) the economic downturn from epidemic loss of productivity and consumption.

The economic output at a given time is considered proportional to the labor participation level at that instant. Following the Cobb–Douglas production rule, with constant capital and labor elasticity b, the production is set at L^b (Douglas, 1976). For a population in optimal health condition, we assume $L_{\max} = 0.9$ and and $b = 0.75$ (e.g., for justification, see Charpentier et al., 2020). The fraction of the population capable of production in the epidemic, $R + S$, is complementary to the drop-out fraction (E+I+D). For each of the two subpopulations α, with $\alpha \in \{0, 1\}$, deploying a specific strategy and undergoing their specific impact of the epidemic, the respective policymaker costs, ECC_α, add up differently

$$\mathrm{ECC}_\alpha = c_{\mathrm{CS}_\alpha} + c_{I_\alpha}\mathcal{J}(I_\alpha, I_{max_\alpha}) + c_{D_\alpha} D_\alpha + c_{L_\alpha} {L_{\max}}^b\left(1 - (1 - E_\alpha - I_\alpha - D_\alpha)^b\right). \tag{8}$$

Each component is controlled by its respective scaling factor, (i) the implementation cost of the control strategy c_{CS_α}, (ii) the cost of disease-related health policy c_{I_α}, (iii) the cost of loss of human life c_{D_α}, and (iv) the epidemic-related economic downturn c_{L_α}. The implementation cost of a control strategy, $c_{\mathrm{CS}_\alpha} \in \mathbb{R}^{9\times 9}$ is split depending on confinement- and vaccination-type and is cumulated when strategies are combined, that is, we assume that there is no interference nor synergy of *cost* due to simultaneous deployment:

$$c_{\mathrm{CS}_0} = \left(0, c_{\mathrm{Css}}, c_{\mathrm{Cwl}}, c_{\mathrm{Vel}}, c_{\mathrm{Vlh}}, c_{\mathrm{Css}} + c_{\mathrm{Vel}}, c_{\mathrm{Css}} + c_{\mathrm{Vlh}}, c_{\mathrm{Cwl}} + c_{\mathrm{Vel}}, c_{\mathrm{Cwl}} + c_{\mathrm{Vlh}}\right)_0^T,$$

and similarly for country-1 (without transposition).[1] Gros et al. (2021) show that the scaling factor c_{I_α} is GDP-dependent for OECD countries, and their study sets this factor to 0.140 on I_α when the value-of-life cost is omitted. To adapt this SIR-based factor to the present SEIRD model which includes a Death-component, a proxy for the ratio I/D of both population segments can be derived from the ratio of the mean transition periods I to R and, I to D, that is, δ_2/ν (see Table 1).

GDP differentiation. The numerical simulation is implemented for two sub-populations with a difference in GDP. With two GDP-differentiated countries adhering to proper control strategies, each suffers a specific *exposed load*, *infection load*, and *death load*, which incur associated costs. The GDP difference also sets a variable cost of intervention for the respective implemented control strategies. In practice, we implemented a parametrized GDP-difference, $\mathrm{GDP}_{\mathrm{diff}} = 0.1$, resulting in an effective differentiated epidemic control cost (ECC) for each nation.[2] This will cause an asymmetry in the ECC cost-based payoff matrix and, subsequently, result in a Nash equilibrium identifying the asymmetrically deployed control strategies. In particular, with subpopulation-1 as reference, subpopulation-0 is corrected for limited resources by a factor $(1 - \mathrm{GDP}_{\mathrm{diff}})$. The cumulated cost of health policy deployment, the value of life, and loss of productivity are scaled to the cost of the implemented control strategy, c_{CS_α}, by a factor $CS_{\mathrm{scale}} = 1.5$. Since no concrete 'vaccination-confinement' scenario is modeled, the relative cost CV_{ratio} of deploying a confinement strategy versus a vaccination strategy is taken over a range of values as well. We estimate the relative deployment cost of confinement (cf. the analysis of Gollier, 2021, on the cost of vaccination) concerning vaccination to range in smaller fractions of the latter; $CV_{\mathrm{ratio}} = .1$, resulting in the respective cost scale factors for confinement, $C_{\mathrm{scale}} = CV_{\mathrm{ratio}} CS_{\mathrm{scale}}$ and, vaccination, $V_{\mathrm{scale}} = CS_{\mathrm{scale}}$. The cost correlation factors are implemented according to the study of Gollier (2021), which is calibrated on French epidemic data in GDP per capita.

$$c_I = 0.140[1 - \mathrm{GDP}_{\mathrm{diff}}, 1], \tag{9}$$

$$c_D = 0.155\,\delta_2/\nu[1 - \mathrm{GDP}_{\mathrm{diff}}, 1], \tag{10}$$

$$c_L = 0.140\,[1 - \mathrm{GDP}_{\mathrm{diff}}, 1], \tag{11}$$

The deployment costs of the basic control strategies are parametrized according to

$$c_{\mathrm{Css}} = C_{\mathrm{scale}}((N_{\mathrm{conn}} - N_{\mathrm{confS}})/N_{\mathrm{conn}})(t_{\mathrm{dur_{Css}}}/t_{\mathrm{dur_{Cwl}}}) \cdot [1 - \mathrm{GDP}_{\mathrm{diff}}, 1], \tag{12}$$

[1] The total ECC payoff matrix, e.g. Table 2, reports country-0 strategies over rows and country-1 strategies over columns.

[2] A wider value range of parameters $\mathrm{GDP}_{\mathrm{diff}}$, CS_{scale} and, CV_{ratio}, with resulting variable Nash Equilibria, are presented in Broekaert et al. (2024c).

Table 2
The average epidemic cost payoff matrix (ECC) for $\mathrm{GDP}_{\mathrm{diff}} = 0.1$; $\mathrm{CS}_{\mathrm{scale}} = 1.5$ and $\mathrm{CV}_{\mathrm{ratio}} = 0.1$ with Nash equilibrium for the Cwl_0-CwlVel_1 control configuration (in purple), for competing two-group control scenarios with partially shuffled-**blocked** group spreading in marginally random social-contact graphs $\mathscr{G}(V_{\mathscr{G}}, E_{\mathscr{G}})$ ($n_{\mathrm{iter}} = 120$, $\mathrm{SD}_{\mathrm{NE}_0}$=0.0075, $\mathrm{SD}_{\mathrm{NE}_1}$=0.0088)..

	No_1	Css_1	Cwl_1	Vel_1	Vlh_1	CssVel_1	CssVlh_1	CwlVel_1	CwlVlh_1
No_0	.3090 / .2784	.3004 / .2766	.2903 / .2759	.3332 / .2780	.4670 / .2778	.2980 / .2761	.4046 / .2756	.2891 / .2755	.3934 / .2750
Css_0	.3068 / .2693	.2986 / .2677	.2902 / .2673	.3310 / .2686	.4631 / .2680	.2935 / .2667	.3974 / .2658	.2871 / .2663	.3903 / .2654
Cwl_0	.3061 / .2603	.2981 / .2601	.2895 / .2596	.3301 / .2596	.4620 / .2589	.2933 / .2590	.3978 / .2580	.2857 / .2585	.3877 / .2574
Vel_0	.3085 / .3044	.2996 / .3025	.2896 / .3016	.3325 / .3038	.4663 / .3037	.2968 / .3018	.4031 / .3013	.2880 / .3010	.3920 / .3005
Vlh_0	.3083 / .4381	.2990 / .4346	.2889 / .4337	.3324 / .4375	.4662 / .4373	.2963 / .4340	.4026 / .4335	.2873 / .4331	.3913 / .4326
CssVel_0	.3063 / .2716	.2975 / .2674	.2889 / .2673	.3303 / .2704	.4624 / .2699	.2919 / .2661	.3957 / .2651	.2855 / .2660	.3885 / .2650
CssVlh_0	.3057 / .3814	.2965 / .3748	.2878 / .3751	.3297 / .3799	.4618 / .3795	.2909 / .3733	.3946 / .3722	.2844 / .3737	.3874 / .3727
CwlVel_0	.3056 / .2635	.2970 / .2616	.2883 / .2603	.3294 / .2624	.4613 / .2617	.2919 / .2602	.3962 / .2591	.2842 / .2590	.3860 / .2579
CwlVlh_0	.3051 / .3713	.2960 / .3683	.2872 / .3659	.3289 / .3699	.4608 / .3692	.2908 / .3666	.3952 / .3655	.2830 / .3644	.3849 / .3633

$$c_{\mathrm{Cwl}} = C_{\mathrm{scale}}((N_{\mathrm{conn}} - N_{\mathrm{confW}})/N_{\mathrm{conn}})(t_{\mathrm{dur}_{\mathrm{Cwl}}}/t_{\mathrm{dur}_{\mathrm{Cwl}}}) \cdot [1 - \mathrm{GDP}_{\mathrm{diff}}, 1], \tag{13}$$

$$c_{\mathrm{Vel}} = V_{\mathrm{scale}} e_{\mathrm{Vel}}(t_{\mathrm{start}_{\mathrm{Vel}}}/t_{\mathrm{start}_{\mathrm{Vlh}}}) \cdot [1 + \mathrm{GDP}_{\mathrm{diff}}, 1], \tag{14}$$

$$c_{\mathrm{Vlh}} = V_{\mathrm{scale}} e_{\mathrm{Vlh}}(t_{\mathrm{start}_{\mathrm{Vlh}}}/t_{\mathrm{start}_{\mathrm{Vlh}}}) \cdot [1 + \mathrm{GDP}_{\mathrm{diff}}, 1]. \tag{15}$$

These costs are GDP-differentiated by country, with region 0 appearing in the first position and region 1 in the second position of the GDP-vector, implementing lower implementation cost in the low-GDP country 0. The cost expression for confinement heuristically compounds the severity of the contact restriction and its duration. It is expressed as the product of the fractional deviation from normal contact N_{conn} and the relative duration of the implemented confinement compared to the duration of long-term confinement $t_{dur_{\mathrm{Cwl}}}$, where $t_{dur_{\mathrm{Css}}}$ denotes the duration of short-term confinement. The cost expression for vaccination control follows a heuristic that compounds the vaccination efficiency e, with $0 \leqslant e \leqslant 1$, acknowledging that developing a highly efficient vaccine with efficiency e_{Vlh} comes at a higher investment cost. It also considers the earliest possible vaccination process start time relative to the later start time of the more efficient vaccine $t_{start_{\mathrm{Vlh}}}$, where $t_{start_{\mathrm{Vel}}}$ denotes the start of the more quickly developed but less efficient vaccine with efficiency e_{Vel}. To independently adjust the heuristic cost expressions of both control measures, separate scale factors C_{scale} for confinement and V_{scale} for vaccination are provided to adjust to real-world implementations.

This formulation allows us to numerically assess the deployment cost of each scenario in the crossing of the various control strategies, Eq. (1). We can now turn to the cost expression in the supply chains.

3.3. Supply chains, performance loss and relocation cost

To model the supply chains, a second network layer is included to identify the supply chain nodes, resulting in the encompassing multiplex graph model. In real-world situations, supply chains are networks of tried and tested providers in each tier; supplying natural resources and labor, and relying on trusted business relationships. In our network model, we subsume these qualities while accepting a procedure of random sampling nodes to assemble a supply chain network. In the present approach, the random sampling procedure of nodes in the supply chain network is only required to derive robust performance metrics that are not biased by network peculiarities (e.g. extreme over- or under-connectivity). These potential biases are further reduced by averaging the performance metrics over a sample set of individual supply chain networks.

The production throughput of the supply chain is impacted by the magnitude of the epidemic – through loss of workforce – and the control strategies – through the conforming of production, transport, and delivery processes with the imposed regulations.

The epidemic-induced *supply chain performance loss* is measured according to the cumulative production metric described in Eq. (16), similar to Broekaert and La Torre (2021). The performance metric of a supply chain records the average longitudinal minimum of $S + R$ over a number of M_{SC} nodes, or segments, of the supply chain network, Eq. (16). It is easily understood that the productivity suffers attrition through lower *Recovered* and *Susceptible* potential of supply chain nodes; when all epidemic disease effects are absent, the sum of these components remains equal to 1. In order to assess the effects of the epidemic and the control regulations on the throughput of the supply chains, a sufficiently large sample of supply chains should be monitored. By averaging this metric over a sample of N_{SC} supply chains, the statistical fluctuations from local network particularities can be mitigated. For the assessment of the supply chains under each regional regulation, it is crucial to distinguish samples for their regional embedding: the nodes of a supply network belonging to only one region, or country, are subject only to their local health policy regulations. In our two-country model, the label '0' will pertain to metrics for 'country-0', and similarly for label '1'. The label '01' is used for a supranational metric, i.e. when nodes are embedded both in country-0 and country-1.

The projected histories S_{Hist} and R_{Hist} of the simulated epidemic are required for the definition of the performance capacity metric

$$\mathrm{cap}_{SC_x} = \frac{1}{M_{SC} N_{SC}} \sum_{k=1,\, l \in \{SC_x\}}^{k=M_{SC}} \min_t (p_{S_k}(t) + p_{R_k}(t))|_l, \quad t \in T, \tag{16}$$

with $x \in \{0, 1, 01\}$ indicating their country of embedding, and each summand over l being one of the N_{SC} supply chains in (inter-)country x. Note that the capacity metric covers the time epoch, T, of the full epidemic wave. For a more detailed temporal covering, a time-slicing corresponding to consecutive waves could be applied.

The metric for the proper performance capacity loss in the supply chain during the parametrized epidemic is given by $\left(1 - \mathrm{cap}_{SC_x}\right)$, and is compounded with the supply chain relocation cost c_{mig}, in the LRC (see Eq. (19) for its definition).

The nodes in the supply chain performance layer inherit the epidemic SEIRD state vectors and are subject to the control strategy of their country. The specific embeddings of the supply chains are sampled separately in each country, or are sampled with a balanced number of nodes from both countries for the supranational supply chains, see Fig. 4.

The control scenario, which renders the optimal costs $\mathrm{ECC}_0^\star$ and $\mathrm{ECC}_1^\star$ for the respective policymakers, as described in Eq. (8), does

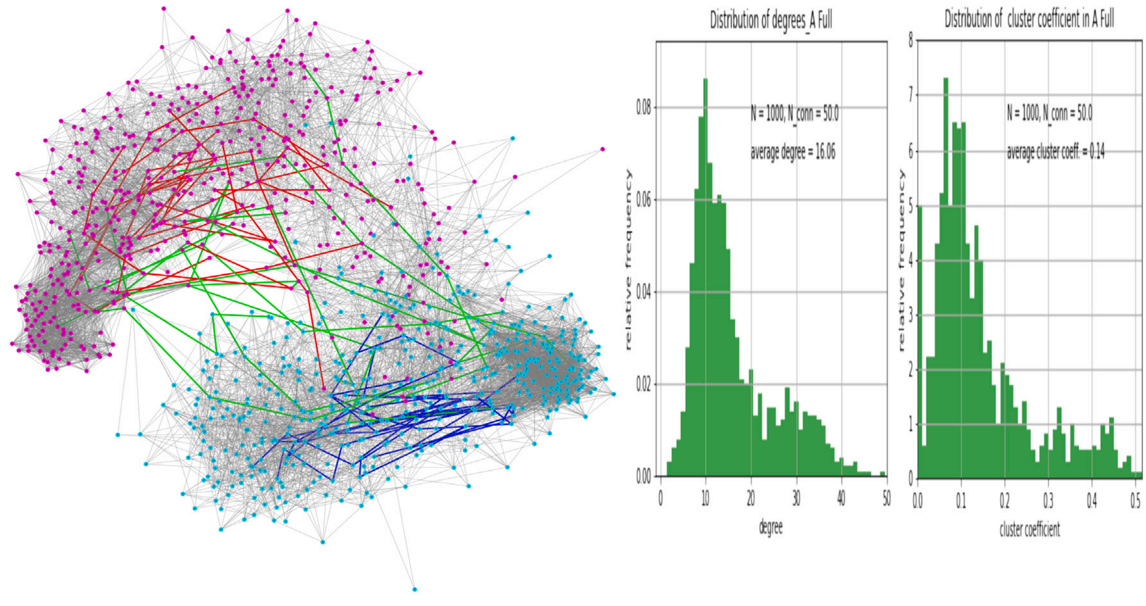

Fig. 4. The multiplex network of supply chains over two distinct block-concentrated but intertwined countries (Magenta vs Cyan) on a marginally randomized social contact graph $\mathscr{G}(V_{\mathscr{G}}, E_{\mathscr{G}})$ according to the adjacency algorithm, $N = 1000$, $N\_conn = 50$, $skew = 0.5$, $orderliness = 0.02$ resulting in a mean degree of 16.06 contacts. For each epidemic rendition, 10 random supply chains are tested in each country (red and blue edges), and another random 10 with supranational covering (lime edges). The degree and cluster coefficient distributions of the shown marginally randomized artificial social-contact graph with high heterogeneity of ego-network size and heavy-tails.

not necessarily coincide with a control scenario that would optimize the capacity loss – cap_{SC} at the Nash equilibrium – of the supply chains. Under the joint control policy following the Nash equilibrium strategy, the manager will assess the firm's resulting costs from supply chain throughput loss and costs related to the possible relocation of supply chain nodes in order to secure a more opportune embedding (see Charpentier et al., 2020; Reddy et al., 2021; Gros et al., 2021; Gollier, 2021).

The cost of supply chain throughput loss. The epidemic attrition of the processing capacity depends on the effectiveness of the local control policy and inflicts a proportional cost for the supply chain manager. Formally, the supply chain capacity loss, $1 - \mathrm{cap}_{SC_x}$, entails a proportional cost of the basic unit B_{cap} and is scaled for the GDP difference. The country's GDP differences typically lead to distinct economic measures such as implementing stimulus packages and financial aid to affected businesses. These further enable the enforcement of social distancing measures, remote working facilitation, or more strict lockdowns without immediately facing severe economic repercussions. The cost of the capacity loss is set to formally depend on the GDP-scaling according to

$$scale_{SC}(\alpha) = [1 - \mathrm{GDP}_{\mathrm{diff}}, 1, 1 - \mathrm{GDP}_{\mathrm{diff}}/2] \tag{17}$$

where $\alpha \in [0, 1, 01]$, i.e. for country-0, country-1, and supranational supply chains between both countries. Notice that the supply chain of 01-type between the two countries is scaled according to the average of both countries (real-world implementations will require adjusted weighting). With the derivation of the local capacity loss due to the epidemic, (see Eq. (16)), the supply chain loss difference on relocation from location α to β is given by:

$$C_{cap}(\alpha, \beta) = B_{cap}(scale_{SC}(\alpha)\ \left(1\text{-}\mathrm{cap}_{SC}(\alpha)\right) - scale_{SC}(\beta)\ \left(1\text{-}\mathrm{cap}_{SC}(\beta)\right)), \tag{18}$$

since the capacity of the epidemically non-impacted supply chain is 1, and deviations due to the epidemic are lost economic activity (see Fig. 5).

The supply chain relocation cost. In addition to throughput loss, the re-designing of a supply chain network (or segments thereof) to another production country by stopping operations at specific nodes to open new ones comes at a basic relocation cost unit B_{mig} and is parametrized to depend on the GDP difference. Given the three possible embeddings 0, 1, and 01 for a supply chain, formally nine possible transition cases are covered in our model. With α the label of the pre-relocation embedding, and β the post-relocation embedding, the nine relocation costs can be concisely noted as

$$C_{mig}(\alpha, \beta) = B_{mig} \cdot \begin{cases} (1 - \delta_{\alpha\beta})\ \left(scale_{SC}(\beta) + \mathrm{GDP}_{\mathrm{diff}}\right), & \alpha = 0 \\ (1 - \delta_{\alpha\beta})\ \ scale_{SC}(\beta), & \alpha = 1 \\ (1 - \delta_{\alpha\beta})\ \left(scale_{SC}(\beta) + \mathrm{GDP}_{\mathrm{diff}}/2\right), & \alpha = 01 \end{cases} \tag{19}$$

where $\delta_{\alpha\beta}$ is the Kronecker delta, $\delta_{\alpha\beta} = 1$ if $\alpha = \beta$, and 0 otherwise. The expression basically accounts for the change in GDP when moving the supply chain from embedding α to β, and adding the cost scale factor B_{mig}.

Under the set condition of the Nash equilibrium control, the managerial decision can be guided by the total cost of relative throughput loss and the cost of relocation (α to β) of the supply chain:

$$\mathrm{LRC}_{SC}(\alpha, \beta) = C_{mig}(\alpha, \beta) + C_{cap}(\alpha, \beta), \tag{20}$$

with $\alpha, \beta \in [0, 1, 01]$ for the appropriate country embedding of the supply chain. In order to generalize our analysis for managerial decision-making on supply chain embedding, the results are calculated for a range of values of $R_{mig/cap} = B_{mig}/B_{cap}$, which is the basic ratio of the relocation cost unit B_{mig} with respect to the total process value of the supply chain production B_{cap}, (see Table 3). This ratio depends on the type of industry branch and the international substitutability of the providers.

All model components are now in place to analyze the potential effects of divergent control strategies on supply chain reconfiguration in the long term (see Fig. 5). In the next section, the model simulations show that control strategies by local policymakers may not align with business goals, as supply chains follow other performance metrics and may operate in supranational configurations.

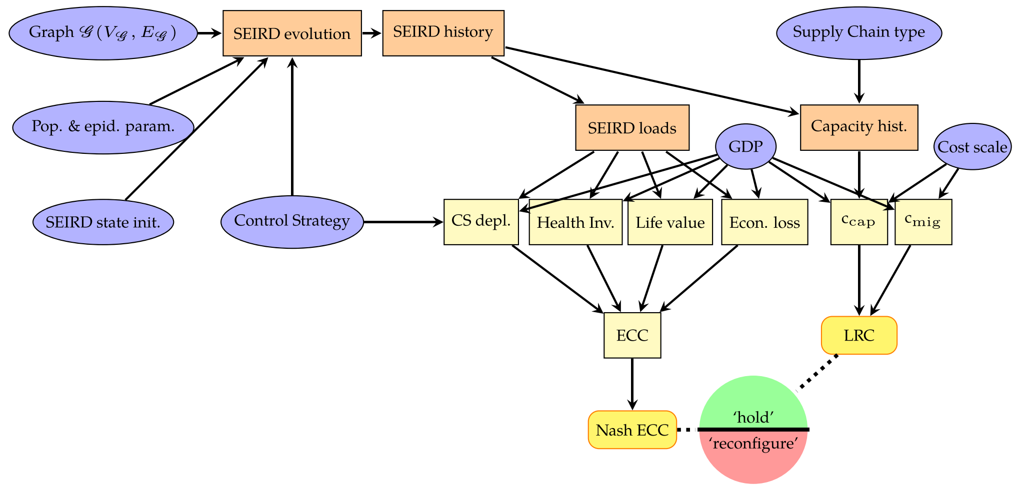

Fig. 5. The methodological flow to analyze supply chain managerial decisions (based on LRC) in response to epidemic control policies (based on ECC). Model inputs (blue ellipses), epidemic dynamics (orange rectangles), and economic and business costs (yellow rectangles) lead to decision factors (yellow rounded) to maintain ('hold') or transform the supply chain configuration ('reconfigure').

Table 3
The LRC, provides the overall cost including supply chain capacity loss *difference* and proper relocation cost, following Eq. (20). The LRC is reported for nine ratios of relocation-cost to basic chain capacity loss, $R_{mig/cap} = 10^{-1}, 15^{-1}, 20^{-1}$ (top tables); $R_{mig/cap} = 25^{-1}, 30^{-1}, 35^{-1}$ (middle); $R_{mig/cap} = 40^{-1}, 45^{-1}, 50^{-1}$ (bottom tables), all under Nash control policy Cwl_0-CwlVel_1. The magnitude of the supply chain relocation cost indicates management possibilities (in purple color) for supply chains originally in country-0 and for supranational 01 configurations ('reconfigure' option). For country-1 supply chains, no reconfiguration is advised in the given epidemic setting ('hold' option).

$R_{mig/cap} = 10^{-1}$			
From \ To	SC_0	SC_1	SC_{01}
SC_0	0	.0366	.0699
SC_1	.1634	0	.1333
SC_{01}	.1301	.0667	0

$R_{mig/cap} = 15^{-1}$			
From \ To	SC_0	SC_1	SC_{01}
SC_0	0	.0066	.0382
SC_1	.1268	0	.0983
SC_{01}	.0951	.0350	0

$R_{mig/cap} = 20^{-1}$			
From \ To	SC_0	SC_1	SC_{01}
SC_0	0	-.0084	0.0224
SC_1	.1084	0	.0808
SC_{01}	.0776	.0192	0

$R_{mig/cap} = 25^{-1}$			
From \ To	SC_0	SC_1	SC_{01}
SC_0	0	-.0174	.0129
SC_1	.0974	0	.0703
SC_{01}	.0671	.0097	0

$R_{mig/cap} = 30^{-1}$			
From \ To	SC_0	SC_1	SC_{01}
SC_0	0	-.0234	.0065
SC_1	.0901	0	.0633
SC_{01}	.0601	.0033	0

$R_{mig/cap} = 35^{-1}$			
From \ To	SC_0	SC_1	SC_{01}
SC_0	0	-.0277	.0020
SC_1	.0849	0	.0583
SC_{01}	.0551	-.0012	0

$R_{mig/cap} = 40^{-1}$			
From \ To	SC_0	SC_1	SC_{01}
SC_0	0	-.0309	-.0014
SC_1	.0809	0	.0546
SC_{01}	.0514	-.0046	0

$R_{mig/cap} = 45^{-1}$			
From \ To	SC_0	SC_1	SC_{01}
SC_0	0	-.0334	-.0040
SC_1	.0779	0	.0517
SC_{01}	.0485	-.0072	0

$R_{mig/cap} = 50^{-1}$			
From \ To	SC_0	SC_1	SC_{01}
SC_0	0	-.0354	-.0061
SC_1	.0754	0	.0493
SC_{01}	.0461	-.0093	0

4. Epidemic, control policy and supply chain simulations

The SEIRSD-dynamical system on the contact-network in Eq. (4), which underlies the epidemic control model and supports the supply chain decision-making, requires a numerical solution procedure because proper analytical solution methods are non-existent for this type of system. The $5 \times N$ system of coupled first-order ODE, Eq. (4), with 'randomized' adjacency matrix (see below) and population heterogeneity, are solved using the Euler-forward method with updated infinitesimal propagator.[3]

Simulation settings. In order to report *robust* outcomes for the epidemic control cost ECC and mitigating strategies, repeated simulations were conducted for which a new contact network was generated and on which all epidemic control configurations were evolved over the long-term. In practice, the simulation experiment covered: $n = 120$ replications (unique networks), each one exposed to 9×9 control strategies (80 controlled epidemics and 1 'free' or uncontrolled epidemic). In each epidemic configuration (120 x 81 in number), 10 supply chains were randomly implemented in each country, and 10 supranational supply chains with their network reaching over the two countries. The size of the contact-network for the two sub-populations was fixed to $N = 1000$ and each supply chain sub-network to $M_{SC} = 6$. Each numerically solved SEIRD-history, e.g. Fig. 6, provides the epidemic data to derive the SEIRD-loads in Eq. (6). The epidemic loads, *averaged* over all replications, serve the relative epidemic cost expressions in Eq. (8) (the latter shows a standard deviation of 0.02 over the experiment, see Table 2). Similarly, for each of these instantiations, the supply chain capacities from Eq. (16), are obtained and inform the average supply chain loss differences in Eq. (18), and the net cost for supply chain re-embedding Eq. (19) (see Table 3 for the compounded results).

[3] The dynamical system Eq. (4) is encoded in Python and the tasks were spread over four different computers – two servers; Jaguar VM and Auckland-UT VM, and two laptops HP i7 1.8 GHz – in batches of 10 graphs during August 2022. Due to computer memory limitations – one SEIRD-history requires 160Mb – only the SEIRD-loads, the adjacency matrix, and the initial infection vector for each unique graph were stored.

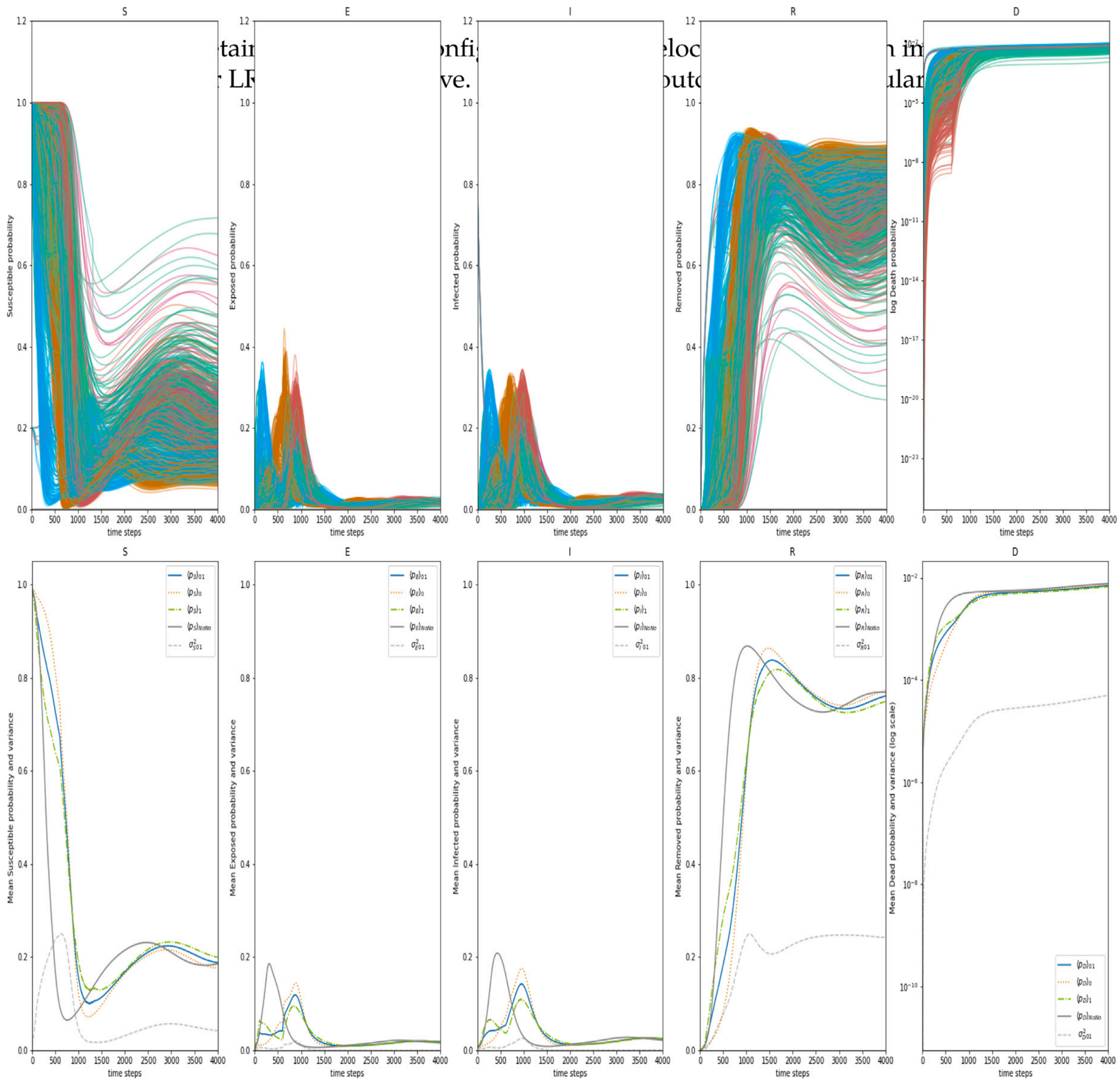

Fig. 6. Example of an epidemic SEIRSD evolution (top panels) in an artificial social-contact network under the Nash equilibrium control strategy Cwl_0-CwlVel_1 with random initial infection seeding, $N_I(0) = 10$, and the corresponding mean-field values and variance (lower panels), with reference values of the No_0-No_1 uncontrolled epidemic (solid gray). Notice the 'flatten the curve' effect (delay and reduce the infection peak) in the third panel for $\langle p_I \rangle$ when comparing the uncontrolled epidemic (solid gray) with the Cwl_0 control (dotted orange) or the CwlVel_1 (dash-dotted green).

Realistic designed contact networks. The simulated social-contact network with high clustering coefficients and high cycle sub-graphs occurrence, for realistic mimicking of the heterogeneous human person-to-person contact network, is re-built for each instantiation (an example population's heterogeneous distribution can be observed in Fig. 4). The algorithm underlying the adjacency is detailed in Broekaert and La Torre (2021) and Broekaert et al. (2022). At its core is the design of a probabilistic adjacency matrix to which a cut-off threshold value can be applied for unconstrained contact $(N - N_{\mathrm{conn}})/N$, or $(N - N_{\mathrm{conf}})/N$ for more stringent confinements $(N_{\mathrm{conn}} > N_{\mathrm{conf}})$.

The realistic SEIRD-parametrization for COVID-19 found in Table 1 follows Korolev (2021), Bjørnstad et al. (2020), Godio et al. (2020), He et al. (2020) and is scaled to the contact-network in line with our study Broekaert et al. (2024c).

Parameter calibration. To transfer epidemic parameter values between compartmental models and graph-based models, scaling is required to adapt values to the average size of ego-networks or the average adjacency degree. The adaptation of the contact parameters from a network model to the corresponding parameters of the compartmental model through node-averaging entails a scaling; $\beta_{\mathcal{G}} = \beta \langle d \rangle_{\mathcal{G}}^{-1}$. In the SEIRSD dynamical equations on the network, Eq. (4), each node aggregates the infection from all its neighbor nodes. The beta-coefficient is therefore scaled relative to the average degree in the network to the exact number of neighbors in an individual's ego-network. Variations of the resulting infection force are discussed in our related studies Broekaert et al. (2022), Broekaert and La Torre (2021). Note that the heterogeneity of the population from random sampling produces a unique system in each simulation run. The SEIRD and social characteristics of each individual are independently sampled according to lognormal distributions around the fixed average values reported in Table 1.

Sanitary control strategy parametrization. The specific implementation of the mitigating control processes requires fixing the control parameters for confinement and vaccination strategies (see also Section 3). The vaccination process, with efficiency e and for $batch$ = 4 random nodes every lag = 10 time steps, transforms the treated nodes according to the weighting according to Eq. (5) into the next time step. The two types of vaccination are parametrized according to: e_{Vel}=.6 for the efficiency, and $start_{\mathrm{Vel}}$=100 of the 'early-&-lower-efficiency' vaccination policy Vel, and e_{Vlh}=.9 and $start_{\mathrm{Vlh}}$=300 for the 'late-&-higher-efficiency' vaccination policy Vlh.

The confinement control strategies from Eq. (1), were parametrized, for Css confinement (strict & short) with $N_{\mathrm{confS}} = 10$, $t_{\mathrm{dur_{Css}}} = 300$, and for the Cwl confinement (weak & long) with $N_{\mathrm{confW}} = 25$, $t_{\mathrm{dur_{Cwl}}} = 500$. Which brings about the contact restrictions in contrast to the normal connectivity $N_{conn} = 50$ in the unconstrained contact graph. A detailed discussion of the effects of this parametrization is given in Broekaert et al. (2024c) For simplified strategy comparison, both confinements were taken to start at $t_{\mathrm{start}_C} = 100$, i.e. at the same time instance.

5. Discussion

5.1. Policymaker's implications

The Payoff Matrix gathers the combinations of the outlined control strategies, leading for each subpopulation to a 9×9 matrix of *epidemic control cost*. Due to the adjacency, the choice of strategy by one public policymaker impacts the outcome of the one followed by the other one. Therefore, the effective total cost can be represented as a two-player *payoff* matrix. The ECC cost from Eq. (8), of each strategic response, is compounded from averaged SEIRD values from identically parametrized epidemics on n = 120 unique social contact graphs. The full payoff matrix for the specific case $\mathrm{GDP_{diff}} = 0.1$; $\mathrm{CS_{scale}} = 1.5$ and $\mathrm{CV_{ratio}} = 0.1$ is reproduced in Table 2.

The Nash equilibrium strategic profile is derived from the policy maker's cost payoff matrix presented in Table 2. In line with our previous study (Broekaert et al., 2024c), with similar parametrization but $\mathrm{GDP_{diff}}$ = 0.1, we find the Nash equilibrium for control is $\mathrm{Cwl_0}$-$\mathrm{CwlVel_1}$, with respectively 0.2585 and 0.2857 cost units given in Table 2. Accordingly, the Nash equilibrium for the public policymaker in country-1 is to deploy early vaccination (with the weaker vaccine) and maintain a graded weak, but longer confinement, while the public policymaker in country-0 only maintains the same 'weak-long' confinement strategy. We recall that the supply chains $\mathrm{SC_0}$ produce in the lower-GDP country ($\mathrm{GDP_{diff}} = 0.1$), while the $\mathrm{SC_1}$ produce in the higher-GDP country.

5.2. Managerial implications

The supply chain performance under controlled epidemic conditions depends on the country in which the supply chain is embedded: country-0 ('embedded in population 0'), country-1 ('embedded in population 1'), or supranational 01('half embedded in populations 0 and 1'). Given the established Nash equilibrium of policies configuration $\mathrm{Cwl_0}$-$\mathrm{CwlVel_1}$, the loss and relocation cost LRC can be tabulated in Table 3. The total relocation cost from Eq. (20), depends on the initial localization ("From") and the possible relocation destination ("To") and is calculated for a range of ratio values, $R_{mig/cap}$, of the relocation cost with respect to the cost of the supply chain capacity loss which is GDP-dependent using Eq. (19). The analysis of total cost LRC in Table 3 indicates that when the *relocation* cost is in the lower ranges, $R_{mig/cap} < 20^{-1}$, the supply chain manager will decide to migrate nodes from country-0 to 1 to optimize costs.

The favorable embedding of supply chains in country-1 corresponds to the improved protection of the supply chain performance under the more extended and costly control strategy that country-1 deployed (resulting in better $(p_{S_k}(t) + p_{R_k}(t))|_l$ values over the supply chain). Notice that even though the total relocation cost LRC was modeled as less costly in country-0, the added mitigation effect of the vaccination campaign in country-1 tips the balance of cost toward relocation from country-0 to country-1. Consequently, the supply chains positioned only in country-1 should be considered to operate under better conditions and their best strategy is to retain their current configuration as no relocation options can improve their LRC cost perspective.These guiding outcomes are particular to the $\mathrm{Cwl_0CwlVel_1}$ control configuration parameters. Given the specific implementation of each parameter-based epidemic, macro-economic parameters, and heterogeneity of contact networks the specific guiding Nash outcome will differ.

5.3. Model sensitivity and limitations

Sensitivity analysis. From the outset, the model's outcome predictions and managerial implications must depend on the specific parametrization, dependencies, and contact architecture. The predictive model aims to correctly assess the outcome dependence on the input data. While the epidemic parameter values were derived from the COVID-19 empiric data and contact degrees were adjusted to literature studies, other economic and business-related parameters were tentatively scaled. The precise parameter values affect the Nash equilibrium as well as the concomitant supply chain strategic decisions. In a previous study, Nash-variability was demonstrated from a psychologically induced change in contact behavior in the population (Broekaert et al., 2024b), and estimated from the *elasticity* of the ECC with respect to its parameters (Broekaert et al., 2024c). To assess the sensitivity of the encompassing model here, an analysis is done for the influence of the network architecture and its heterogeneous populations, and for variations of the economic parameters.

(i) The variable structure of connected ego-networks, the heterogeneous attribution of disease-related parameters throughout the population and, the random seeding of initial infectious individuals in each iteration lead to a specific severity and development of the disease epidemic. The variations of the contact network and population properties will lead to Nash equilibria of the ECC different from the graph-*averaged* one, $\mathrm{Cwl_0}$-$\mathrm{CwlVel_1}$, Table 2. In the set of unaggregated instances of the population network, this average-based Nash equilibrium occurs in just 42.5% of the instances. Variations of the network will see confinement switch between Cwl and Css in both countries, but never will the Css variant be simultaneously deployed. Also, both countries will opt – or not – for vaccination variant Vel, but neither will opt for type Vlh (see Fig. 7).

(ii) The Epidemic Control Cost expression, Eq. (8), depends besides the SEIRD-loads also on the specific values of the economic parameters. The implemented values are therefore decisive in the resulting Nash strategic profiles. The variability of the ECC can be estimated from the *elasticity* with respect to the parameters in the expression, Eq. (8) (see Broekaert et al., 2024a). Formally the ECC satisfies, $\mathrm{ECC} = \sum_\lambda C_\lambda$ with $C_\lambda(\alpha \cdot \lambda) = \alpha \cdot C_\lambda(\lambda)$, leading to the parameter-λ elasticity of $\epsilon_\lambda = \frac{C_\lambda}{C}$. The variation of, L_{Max}, leads to the labor-elasticity of cost $\epsilon_L = b\frac{C_L}{C}$, with variations of about 2% to 12% in our simulations, Table 2. This variability may induce shifts in the optimal Nash strategy. To analyze the sensitivity of the Nash Equilibrium, a shift of the magnitude $\pm 10\%$ of a parameter's standard value was implemented. For each adapted parameter value, the Nash equilibrium was identified from the updated game matrices. The variability of the Nash strategic profiles is rather robust for these variations: only Country-0 adopts the supplementary Vel vaccination control for an increase of the parameters c_D, L_{Max} and b (Cobb), while a decrease of c_I results in the same strategic adaptation, Table 4.

More formal **method limitations** stem from the common issue of lacking detailed real-world system information. This typically impedes the development of a fully individual-based fine-grained model. E.g., in a real-world epidemic situation, neither the population's contact-network nor their specific SEIRD-characteristics are known; network simulations are then necessary to obtain robust outcomes on health

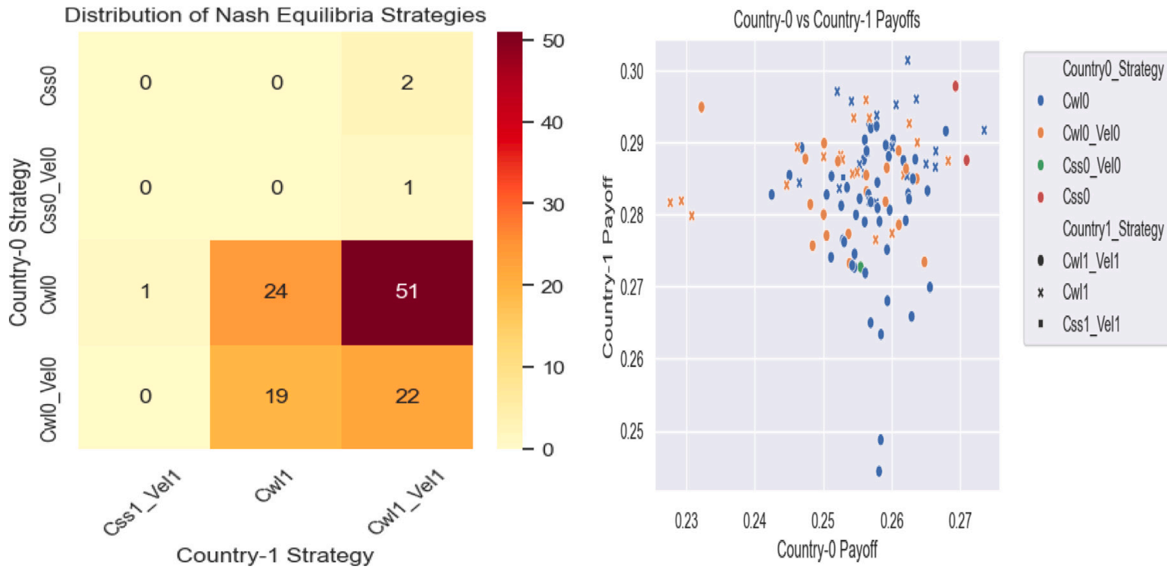

Fig. 7. Network and population induced deviations of the average Nash profile occur as Cwl_0-Cwl_1 (20.0%), CwlVel_0-CwlVel_1 (18.3%), CwlVel_0-Cwl_1 (15.8%) and rarely as Css_0-CwlVel_1 (1.7%) or CssVel_0-CwlVel_1 (< 1%) (left panel). Purely from network and population variation, country-0 incurs an average ECC of 0.256, varying in the range [0.228, 0.273], while Country-1 incurs a higher average ECC of 0.284 with [0.244, 0.301] range variation (right panel, hue from country-0, style from country-1).

Table 4
Sensitivity of the ECC Nash Equilibrium for economic parameter variations about GDP_diff = .1, c_I = .14, c_D = .155, L_{Max} = .9, b = .75. Parameters with changed Nash profiles for ±10% variations are marked in purple.

Nash		GDP_diff	c_I	c_D	L_{Max}	b (Cobb)
-10%	Strategy	$\mathrm{Cwl}_0\mathrm{CwlVel}_1$	$\mathrm{CwlVel}_0\mathrm{CwlVel}_1$	$\mathrm{Cwl}_0\mathrm{CwlVel}_1$	$\mathrm{Cwl}_0\mathrm{CwlVel}_1$	$\mathrm{Cwl}_0\mathrm{CwlVel}_1$
	values	(.2614,.2857)	(.2485,.2728)	(.241,.2686)	(.2451,.2721)	(.2559,.2836)
+10%	Strategy	$\mathrm{Cwl}_0\mathrm{CwlVel}_1$	$\mathrm{Cwl}_0\mathrm{CwlVel}_1$	$\mathrm{CwlVel}_0\mathrm{CwlVel}_1$	$\mathrm{CwlVel}_0\mathrm{CwlVel}_1$	$\mathrm{CwlVel}_0\mathrm{CwlVel}_1$
	value	(.2556,.2857)	(.2669,.2972)	(.2744,.3012)	(.271,.2975)	(.2608,.2862)

strategies and managers' supply chain decisions. From a computational perspective, the size of detailed international networks will require considerable computation power. This issue of tractability further increases when the spectrum of control policies is further increased. Finally, the multiplex system could be expanded to include the possibility of changes in the control policies triggered by induced supply chain relocation and capacity loss. While possible in principle, such a model requires again an extended game matrix of strategies based on realistic supply chain cost response from industry.

5.4. Practical and generalized applications

The practical applicability of the decision-supporting model is shortly examined in two literature-based case studies (see further details in Broekaert et al., 2024a). The model's incorporation for optimizing supply chain throughput during epidemics across national boundaries is demonstrated at the hand of these cases by comparative analysis between the actual démarche and our model's recommendations.

The **first case study** by Burgos and Ivanov (2021) on COVID-19 pandemic effects on German food retail supply chains utilizes a discrete-event simulation model in anyLogistix. A network structure examined comprised thirty suppliers across ten product categories, with distribution facilitated through three centers in Germany serving twenty-eight supermarket locations across five European nations. It was observed that supply chain performance was predominantly affected by demand fluctuations and supplier closures, while transportation disruptions were found to be less impactful. The proposed individual-based network model with geographic embedding could be utilized to enhance the analysis of supranational food retail supply chains. In their setup concerning supplier factory shutdowns, a more granular assessment of labor availability could be achieved through the integration of disease-based temporal and spatial impacts. Regional variations in control strategies could thus be incorporated, enabling comparative analysis of network configuration alternatives. A setup focused on border control disruptions could be enhanced through the incorporation of our model's capacity to account for reduced cross-border virus transmission. The **second case study** by Shen and Sun (2023) studies JD.com's supply chain management during COVID-19. The company's Wuhan distribution center, serving 120 warehouses across multiple provinces, was impacted by lockdown measures. Through quantitative operational data analysis, it was demonstrated how supply chain management adaptations were implemented in response to the event's demands and logistical challenges. A data-driven network redesign allowed to bypass non-functional pathways and facilities. Our multiplex network ontology could allow to analyze the cost-based reconfigurations, with specific adaptations through component substitution guided by regional control measures.

In practice, supply chain reconfiguration implies **timeframe-related** processes, including production facility relocation between countries, supplier negotiations, and prior commitment resolutions. Two complementary options are considered regarding the timeframe of supply chain reconfiguration as projected by our decision optimization procedure.

Concretely, a *single-wave* epidemic timeframe is addressed here by our decision support model implementation, whereby the real-world agility of specific businesses and industries may be challenged. In practice, the timeframe of diverging control strategies in general – e.g. on economic or socio-political grounds – between policymakers like international trade agreements, regional investment plans or stimulating fiscal spaces, may effectively offer a *more extended* temporal perspective for supply chain reconfiguration. Nevertheless, the compelling industry case of JD.com, documented by Shen and Sun (2023), reports the supply chain reconfiguration process during the COVID-19 pandemic in China. Through this case, it is demonstrated how supply chains can be reconfigured during epidemic timeframes, supporting the practical application of our proposed decision-making method.

When multiple episodes of diverging control strategies are encountered, supply chain performance can be longitudinally assessed through our decision support method, as detailed in Broekaert et al. (2024a). The timeframe for reconfigurations can be extended to cover multi-stage impacting events through the Longitudinal Service Level metric, which is used to monitor the Service Level across socio-economic shocks. In practice, the Service Level is defined by the percentage of customer demand that is met without delay from available inventory, in our model it is heuristically correlated with supply chain nodes' time spent in Recovered and Susceptible states. The harmonic mean is utilized to aggregate average activity levels across three consecutive epidemic waves, emphasizing the weakest values in activity concatenation. Wider timeframes are thus addressed through the LSL metric for supply chain reconfiguration, maintaining alignment with subsequent Nash control strategy profiles.

For a **generalized approach** using our model, a network architecture and dynamics can be formally adapted to various instances e.g., (i) the spread of financial distress among financial institutions, banks, and firms, due to contagion effects during a financial crisis, (ii) the adoption of new products, or technologies within a population to forecast market penetration, (iii) the diffusion of opinions, beliefs, and behaviors within populations to understand trends in consumer or political choices, and (iv) systems of transportation undergoing regional upgrades and affecting economic features as e.g. property values and job availability. The ensuing Nash Equilibria may then be derived from the strategy pay-off matrix between the various stakeholders. The latter is defined again according to its use case.

Inter-regional divergences in fiscal stimulation policies will alter the attractiveness of regional production locations, and distribution centers — e.g., alleviating the factor of less efficient transportation routes. Also, differing environmental zoning regulations and land-use policies that affect the possibility of manufacturing processes and locations for facilities will place regional politicians or decision-makers in competing positions. Finally, international regulatory differences concerning, tariffs, labor laws and wage regulations, technical product standards, environmental regulations, intellectual property laws and data privacy laws, amongst various other precepts, all constitute a possibility for competitive decision-making.

In principle, finding the induced Nash Equilibrium follows from simulating the network diffusion dynamics for all possible combinations of the mitigation policies. Subsequently, the established Nash strategy profile then sets the context in which a given supply chain's capacity change and relocation cost LRC can be figured.

6. Conclusions

The combined supply chain and epidemic network model elucidates how supply chains are modified to accommodate varying health control policies implemented in adjacent countries or regions. Divergent epidemic control measures result in varied supply chain performances, contingent on the region of activity. Initially, the model demonstrates how public policymakers assess health policies by considering factors such as the cost of sanitary control strategies, the expenditure and deployment costs of epidemic-related policies, the value of human life, and the economic productivity losses related to epidemics.

The Nash equilibrium, derived from each region's or country's health policy and its impact on population health, determines the respective levels of potential productive activity. Consequently, managers strategically modify their supply networks accordingly. A novel aspect of our control policy model over differentiated regions is the ensuing predictive capability for cost-based supply chain reconfiguration. Although based on numerical simulations of designed-random realistic social-contact networks, the method can, in principle, be applied to real-world configurations with divergent control policies. In practice, this will require the implementation of the multiplex system spanning the network layer of the *supply chains* over the layer which implements the diffusion of the epidemic or any other localized network of production affecting features — e.g. local weather impact, local employment levels, or local carbon emission.

By considering a multiplex network, comprising a resource network layer where local policy regulations exert a local impact, and a supply chain network layer of firms reliant on these local resources, the method monitors how control policies impact local economies, including the reconfiguration of supply networks. In a detailed example case, realistic and robust managerial metrics for supply chains under a SEIRSD-epidemic spreading over two neighboring countries are derived. The analytically intractable epidemic dynamics on highly heterogeneous populations are addressed through repeated numeric simulations: 120 replications, each covering a 9×9 crossed control strategy matrix, with 10 supply chains randomly implemented in both countries and 10 supranational supply chains across the two countries.

The model considers two separate populations from adjacent countries or regions with differing GDP per capita (see Fig. 4). This asymmetry in GDP per capita ultimately gives rise to an asymmetric Nash equilibrium strategy of control policies followed by the two countries — the scenario Cwl_0-CwlVel_1, as described in Section 4. In general, other regional or national economic or socio-political policies can be considered that will result in a similar strategic matrix game. Subsequently, the cost of supply chain capacity loss is obtained from the underlying resource network information, including the potential cost of supply chain relocations (LRC). This metric effectively clarifies the policy conditions under which a supply chain's performance can be optimized by adapting the network layout across different countries. Our method hence aids managers in adapting their networks by establishing new supplier or distribution relationships in different countries – pruning and creating new nodes – thereby preserving the viability of their supply chains. In this way, we validate from a different angle the results obtained in the work of Ivanov and Dolgui (2020), Ivanov et al. (2023) and Brusset et al. (2022, 2023).

In particular, the example case shows that improved epidemic mitigation in the relatively higher-GDP region ('country-1') better protects the supply chain throughput performance. Despite the lower implicit relocation cost to the lower-GDP country, the mitigation effect of the improved control (here 'Vel_1'-type vaccination in country-1) encourages supply chain relocation there.

The present study considers only two countries and a limited number of sampled supply networks due to computational constraints and for clarity of the argument. The model can be extended to accommodate more countries, more supply networks, and longer time periods; the main constraints are the availability of data and computational power. In real-world scenarios, a true population's contact-network – e.g. their specific SEIRD-characteristics – or the underlying network of production-affecting features are often not fully known; necessitating network simulations to obtain robust outcomes for the various control strategies and managers' supply chain decisions.

We believe that our encompassing model can be suitably adapted to specific countries and control policy configurations. For case-specific adaptations, once provided with the specific supply chain parameters including node topology and their distribution over the countries, and costs, the system is fully defined, enabling managers to obtain information on optimal reconfigurations based on the control policies and the characteristics of the location-based network of production. These modifications of the supply network necessitate knowledge of existing alternative possibilities in the production or distribution environment.

Our proposed decision-supporting model imparts actionable insights on the part of policymakers, supply chain managers, and their common concerns. While epidemic modeling currently is a core instrument in the policymaker's decision-making, our multi-player perspective of divergent stakeholders can provide added insight;

- Policymakers should calibrate their control strategies based on their country's economic capacity and cost of control operations in comparison to *interconnected* countries. Unilateral actions may be less effective due to network interdependencies with GDP-differentiated countries and their derived control strategies.

The supply chain manager's perspective hinges on the precise quantification of losses incurred in the supply chain landscape and cost of reconfigurations;

- Managers should map supply network alternative configurations for production capabilities, operation costs, and impacted processes under different (GDP-differentiated) regional control policies, and then monitor the reconfiguration options based on both immediate incurred costs and for long-term regional reconfigurations.

The extensive data-based foundation of this type of decision-making model requires in general a thorough quantitative representation of the full system ontology;

- Implement robust data collection and monitoring systems to track labor capacity metrics, contact patterns, and the performance of supply chain nodes. An extensive range of policies crossed with foreign policymaker's options then need to be simulated for optimal epidemic outcomes of epidemic models and inform supplier substitutability.

The core method in our model then leads the various policymakers into establishing the Nash equilibrium of mitigating policies. Here, underlying diffusion dynamics on population networks revealed the economic and health outcomes of the control policies. The supply chain managers and entrepreneurs then optimize their supply networks – in terms of production – within the setting of the Nash strategy profile. In general, an induced Nash Equilibrium from all crossed control strategies provides the context from which the supply chain's cost of relocation and supply chain capacity loss (LRC) can be calculated and hence explains the policymaker's hand in setting the boundaries for supranational supply chain dynamics.

CRediT authorship contribution statement

Jan B. Broekaert: Writing – review & editing, Writing – original draft, Visualization, Validation, Software, Methodology, Investigation, Formal analysis, Data curation, Conceptualization. **Davide La Torre:** Writing – review & editing, Writing – original draft, Supervision, Resources, Project administration, Methodology, Funding acquisition, Conceptualization. **Faizal Hafiz:** Writing – review & editing, Software, Methodology, Conceptualization. **Xavier Brusset:** Writing – review & editing, Writing – original draft, Project administration, Methodology, Conceptualization.

Declaration of competing interest

The authors declare that they have no known competing financial interests or personal relationships that could have appeared to influence the work reported in this paper.

Data availability

The data is available at the OSF repository.

References

Ajmal, M.M., Khan, M., Shad, M.K., 2021. The global economic cost of coronavirus pandemic: current and future implications. Public Adm. Policy 24 (3), 290–305.

Alikhani, R., Eskandarpour, M., Jahani, H., 2023. Collaborative distribution network design with surging demand and facility disruptions. Int. J. Prod. Econ. 262, 108912.

Amir, R., Boucekkine, R., 2022. Introduction to the special issue on new insights into economic epidemiology: Theory and policy. J. Public Econ. Theory 24 (5), 861–872.

Ardolino, M., Bacchetti, A., Ivanov, D., 2022. Analysis of the COVID-19 pandemic's impacts on manufacturing: a systematic literature review and future research agenda. Oper. Manag. Res..

Aum, S., Lee, S.Y.T., Shin, Y., 2021. Inequality of fear and self-quarantine: Is there a trade-off between GDP and public health? J. Public Econ. 194, 104354.

Berger, N., Schulze-Schwering, S., Long, E., Spinler, S., 2023. Risk management of supply chain disruptions: An epidemic modeling approach. European J. Oper. Res. 304 (3), 1036–1051.

Bertozzi, A.L., Franco, E., Mohler, G., Short, M.B., Sledge, D., 2020. The challenges of modeling and forecasting the spread of COVID-19. Proc. Natl. Acad. Sci. 117 (29), 16732–16738.

Bjørnstad, O.N., Shea, K., Krzywinski, M., Altman, N., 2020. The SEIRS model for infectious disease dynamics. Nature Methods 17 (6), 557–558.

Borgatti, S., Halgin, D.S., 2011. Network theorizing. Organ. Sci. 22 (5), 1168–1181.

Boucekkine, R., Carvajal, A., Chakraborty, S., Goenka, A., 2021. The economics of epidemics and contagious diseases: An introduction. J. Math. Econom. 93, 102498.

Broekaert, J., Hafiz, F., Jayaraman, R., La Torre, D., 2024a. Managing resilience and viability of supranational supply chains under epidemic control scenarios. Omega 103234.

Broekaert, J.B., La Torre, D., 2021. A vector logistic dynamical approach to epidemic evolution on interacting social-contact and production-capacity graphs. In: Dolgui, A., Bernard, A., Lemoine, D., von Cieminski, G., Romero, D. (Eds.), Advances in Production Management Systems. Artificial Intelligence for Sustainable and Resilient Production Systems. Springer International Publishing, Cham, pp. 13–22.

Broekaert, J.B., La Torre, D., Hafiz, F., 2022. Competing control scenarios in probabilistic SIR epidemics on social-contact networks.. Ann. Oper. Res. 1–24.

Broekaert, J.B., La Torre, D., Hafiz, F., 2024b. The impact of the psychological effect of infectivity on Nash-balanced control strategies for epidemic networks. Ann. Oper. Res..

Broekaert, J.B., La Torre, D., Hafiz, F., Repetto, M., 2024c. A comparative cost assessment of coalescing epidemic control strategies in heterogeneous social-contact networks. Comput. Oper. Res. 167, 106680.

Brusset, X., Davari, M., Kinra, A., Torre, D.L., 2022. Modelling ripple effect propagation and global supply chain workforce productivity impacts in pandemic disruptions. Int. J. Prod. Res. 1–20.

Brusset, X., Ivanov, D., Jebali, A., La Torre, D., Repetto, M., 2023. A dynamic approach to supply chain reconfiguration and ripple effect analysis in an epidemic. Int. J. Prod. Econ. 263, 108935.

Burgos, D., Ivanov, D., 2021. Food retail supply chain resilience and the COVID-19 pandemic: A digital twin-based impact analysis and improvement directions. Transp. Res. Part E: Logist. Transp. Rev. 152, 102412.

Charpentier, A., Elie, R., Laurière, M., Tran, V.C., 2020. COVID-19 pandemic control: balancing detection policy and lockdown intervention under ICU sustainability*. Math. Model. Nat. Phenom. 15, 57.

Chen, K., Pun, C.S., Wong, H.Y., 2023. Efficient social distancing during the COVID-19 pandemic: Integrating economic and public health considerations. European J. Oper. Res. 304 (1), 84–98.

Choi, T.-M., 2021. Fighting against COVID-19: What operations research can help and the sense-and-respond framework. Ann. Oper. Res..

Darabi Sahneh, F., Scoglio, C., Van Mieghem, P., 2013. Generalized epidemic mean-field model for spreading processes over multilayer complex networks. IEEE/ACM Trans. Netw. 21 (5), 1609–1620.

Das, S., Bose, I., Sarkar, U.K., 2023. Predicting the outbreak of epidemics using a network-based approach. European J. Oper. Res. 309 (2), 819–831.

Dobson, A., Ricci, C., Boucekkine, R., Gozzi, F., Fabbri, G., Loch-Temzelides, T., Pascual, M., 2023. Balancing economic and epidemiological interventions in the early stages of pathogen emergence. Sci. Adv. 9 (21), eade6169.

Dolgui, A., Gusikhin, O., Ivanov, D., Li, X., Stecke, K., 2023. A network-of-networks adaptation for cross-industry manufacturing repurposing. IISE Trans. 1–17.

Dolgui, A., Ivanov, D., Sokolov, B., 2020. Reconfigurable supply chain: the X-network. Int. J. Prod. Res. 58 (13), 4138–4163.

Douglas, P.H., 1976. The cobb-douglas production function once again: Its history, its testing, and some new empirical values. J. Political Econ. 84 (5), 903–915.

El Baz, J., Ruel, S., 2021. Can supply chain risk management practices mitigate the disruption impacts on supply chains' resilience and robustness? Evidence from an empirical survey in a COVID-19 outbreak era. Int. J. Prod. Econ. 233, 107972.

Eryarsoy, E., Shahmanzari, M., Tanrisever, F., 2023. Models for government intervention during a pandemic. European J. Oper. Res. 304 (1), 69–83.

Fagiolo, G., 2020. Assessing the impact of social network structure on the diffusion of coronavirus disease (COVID-19): A generalized spatial SEIRD model.

Fan, C., Jiang, X., Lee, R., Mostafavi, A., 2022a. Data-driven contact network models of COVID-19 reveal trade-offs between costs and infections for optimal local containment policies. Cities 128, 103805.
Fan, J., Yin, Q., Xia, C., Perc, M., 2022b. Epidemics on multilayer simplicial complexes. Proc. R. Soc. A: Math. Phys. Eng. Sci. 478 (2261), 20220059.
Farahani, R.Z., Ruiz, R., Van Wassenhove, L.N., 2023. Introduction to the special issue on the role of operational research in future epidemics/ pandemics. European J. Oper. Res. 304 (1), 1–8.
Freiberger, M., Grass, D., Kuhn, M., Seidl, A., Wrzaczek, S., 2022. Chasing up and locking down the virus: Optimal pandemic interventions within a network. J. Public Econ. Theory 24 (5), 1182–1217.
Godio, A., Pace, F., Vergnano, A., 2020. SEIR modeling of the Italian epidemic of SARS-CoV-2 using computational swarm intelligence. Int. J. Environ. Res. Public Heal. 17 (10), 3535.
Gollier, C., 2021. The welfare cost of vaccine misallocation, delays and nationalism. J. Benefit- Cost Anal. 12 (2), 199–226.
Grabisch, M., Rusinowska, A., Venel, X., 2022. Diffusion in large networks. J. Econom. Dynam. Control 139, 104439.
Gros, C., Valenti, R., Schneider, L., Valenti, K., Gros, D., 2021. Containment efficiency and control strategies for the corona pandemic costs. Sci. Rep. 11 (1), 6848.
Großmann, G., Backenköhler, M., Wolf, V., 2021. Heterogeneity matters: Contact structure and individual variation shape epidemic dynamics. PLOS ONE 16 (7), 1–19.
He, S., Peng, Y., Sun, K., 2020. SEIR modeling of the COVID-19 and its dynamics. Nonlinear Dynam. 101, 1667–1680.
Hevia, C., Macera, M., Neumeyer, P.A., 2022. Covid-19 in unequal societies. J. Econom. Dynam. Control 140, 104328.
Hille, K., 2021. Taiwan's Covid-19 outbreak spreads to chip companies. Financ. Times.
Hosseini, S., Ivanov, D., 2019. A new resilience measure for supply networks with the ripple effect considerations: a Bayesian network approach. Ann. Oper. Res. S.I. Design and Management of Humanitarian Supply Chains, 1.
Ivanov, D., 2020. Predicting the impacts of epidemic outbreaks on global supply chains: A simulation-based analysis on the coronavirus outbreak (COVID-19/SARS-CoV-2) case. Transp. Res. Part E: Logist. Transp. Rev. 136, 101922.
Ivanov, D., 2021. Supply chain viability and the COVID-19 pandemic: a conceptual and formal generalisation of four major adaptation strategies. Int. J. Prod. Res. 59 (12), 3535–3552.
Ivanov, D., 2023. Intelligent digital twin (iDT) for supply chain stress-testing, resilience, and viability. Int. J. Prod. Econ. 263, 108938.
Ivanov, D., 2024. Supply chain resilience: Conceptual and formal models drawing from immune system analogy. Omega 127, 103081.
Ivanov, D., Dolgui, A., 2020. Viability of intertwined supply networks: extending the supply chain resilience angles towards survivability. a position paper motivated by COVID-19 outbreak. Int. J. Prod. Res. 58 (10), 2904–2915.
Ivanov, D., Dolgui, A., Blackhurst, J.V., Choi, T.-M., 2023. Toward supply chain viability theory: from lessons learned through COVID-19 pandemic to viable ecosystems. Int. J. Prod. Res. 61 (8), 2402–2415.
Ivanov, D., Sokolov, B., Chen, W., Dolgui, A., Werner, F., Potryasaev, S., 2020. A control approach to scheduling flexibly configurable jobs with dynamic structural-logical constraints. IISE Trans. 53 (1), 21–38.
Jackson, J.K., Weiss, M.A., Schwarzenberg, A.B., Nelson, R.M., Sutter, K.M., Sutherland, M.D., 2021. Global economic effects of COVID-19. (R46270), Congressional Research Service.
Jiang, J., Ma, J., Chen, X., 2024. Multi-regional collaborative mechanisms in emergency resource reserve and pre-dispatch design. Int. J. Prod. Econ. 270, 109161.
Keeling, M.J., Eames, K.T., 2005. Networks and epidemic models. J. R. Soc. Interface 2 (4), 295–307.
Kermack, W., McKendrick, A., 1927. A contribution to the mathematical theory of epidemics. Proc. R. Soc. Lond. Ser. A 115 (772), 700–721.
Kinra, A., Ivanov, D., Das, A., Dolgui, A., 2020. Ripple effect quantification by supplier risk exposure assessment. Int. J. Prod. Res. 58 (18), 5559–5578.
Korolev, I., 2021. Identification and estimation of the SEIRD epidemic model for COVID-19. J. Econometrics 220 (1), 63–85.
Levin, E.G., Lustig, Y., Cohen, C., Fluss, R., Indenbaum, V., Amit, S., Doolman, R., Asraf, K., Mendelson, E., Ziv, A., Rubin, C., Freedman, L., Kreiss, Y., Regev-Yochay, G., 2021. Waning immune humoral response to BNT162b2 Covid-19 vaccine over 6 months. N. Engl. J. Med. 385 (24), e84.
Li, C.-H., Tsai, C.-C., Yang, S.-Y., 2014. Analysis of epidemic spreading of an SIRS model in complex heterogeneous networks. Commun. Nonlinear Sci. Numer. Simul. 19 (4), 1042–1054.
Li, Y., Zobel, C.W., 2020. Exploring supply chain network resilience in the presence of the ripple effect. Int. J. Prod. Econ. 228, 107693.
Llaguno, A., Mula, J., Campuzano-Bolarin, F., 2021. State of the art, conceptual framework and simulation analysis of the ripple effect on supply chains. Int. J. Prod. Res..
Lofvers, M., 2020. Three-quarters of European supply chains are negatively impacted by coronavirus. Supply Chain Movement, Digital Magazine,
MacIntyre, C.R., Costantino, V., Trent, M., 2021. Modelling of COVID-19 vaccination strategies and herd immunity, in scenarios of limited and full vaccine supply in NSW, Australia. Vaccine.
Mishra, D., Dwivedi, Y.K., Rana, N.P., Hassini, E., 2019. Evolution of supply chain ripple effect: a bibliometric and meta-analytic view of the constructs. Int. J. Prod. Res. 59 (1), 129–147.
Nagurney, A., 2021a. Optimization of supply chain networks with inclusion of labor: Applications to COVID-19 pandemic disruptions. Int. J. Prod. Econ. 235, 108080.
Nagurney, A., 2021b. Supply chain game theory network modeling under labor constraints: Applications to the Covid-19 pandemic. European J. Oper. Res. 293 (3), 880–891.
Nagurney, A., Flores, E.A., Soylu, C., 2016. A generalized Nash equilibrium network model for post-disaster humanitarian relief. Transp. Res. Part E: Logist. Transp. Rev. 95, 1–18.
Newman, M., 2018. Networks. Oxford University Press.
Nikolopoulos, K., Punia, S., Schäfers, A., Tsinopoulos, C., Vasilakis, C., 2021. Forecasting and planning during a pandemic: COVID-19 growth rates, supply chain disruptions, and governmental decisions. European J. Oper. Res. 290 (1), 99–115.
Nuss, P., Graedel, T., Alonso, E., Carroll, A., 2016. Mapping supply chain risk by network analysis of product platforms. Sustain. Mater. Technol. 10, 14–22.
Ottaviano, S., Bonaccorsi, S., 2021. Some aspects of the Markovian SIRS epidemic on networks and its mean-field approximation. Math. Methods the Apllied Sci. 44 (6), 4952–4971.
Ouardighi, F.E., Khmelnitsky, E., Sethi, S.P., 2022. Epidemic control with endogenous treatment capability under popular discontent and social fatigue. Prod. Oper. Manage..
Park, Y.W., Blackhurst, J., Paul, C., Scheibe, K.P., 2021. An analysis of the ripple effect for disruptions occurring in circular flows of a supply chain network. Int. J. Prod. Res. 1–19.
Pastor-Satorras, R., Castellano, C., Van Mieghem, P., Vespignani, A., 2015. Epidemic processes in complex networks. Rev. Modern Phys. 87, 925–979.
Paul, S.K., Moktadir, M.A., Sallam, K., Choi, T.-M., Chakrabortty, R.K., 2021. A recovery planning model for online business operations under the COVID-19 outbreak. Int. J. Prod. Res. 1–23.
Peng, K., Lu, Z., Lin, V., Lindstrom, M.R., Parkinson, C., Wang, C., Bertozzi, A.L., Porter, M.A., 2021. A multilayer network model of the coevolution of the spread of a disease and competing opinions.
Plazas, A., Malvestio, I., Starnini, M., Díaz-Guilera, A., 2021. Modeling partial lockdowns in multiplex networks using partition strategies. Appl. Netw. Sci. 6 (1), 27.
Prasse, B., Devriendt, K., Van Mieghem, P., 2021. Clustering for epidemics on networks: A geometric approach. Chaos: An Interdiscip. J. Nonlinear Sci. 31 (6), 063115.
Reddy, K.P., Shebl, F.M., Foote, J.H.A., Harling, G., Scott, J.A., Panella, C., Fitzmaurice, K.P., Flanagan, C., Hyle, E.P., Neilan, A.M., Mohareb, A.M., Bekker, L.-G., Lessells, R.J., Ciaranello, A.L., Wood, R., Losina, E., Freedberg, K.A., Kazemian, P., Siedner, M.J., 2021. Cost-effectiveness of public health strategies for COVID-19 epidemic control in South Africa: a microsimulation modelling study. Lancet Glob. Heal. 9 (2), e120–e129.
Reicher, S., Stott, C., 2020. On order and disorder during the COVID-19 pandemic. Br. J. Soc. Psychol. 59 (3), 694–702.
Rezapour, S., Baghaian, A., Naderi, N., Sarmiento, J.P., 2023. Infection transmission and prevention in metropolises with heterogeneous and dynamic populations. European J. Oper. Res. 304 (1), 113–138.
Rozhkov, M., Ivanov, D., Blackhurst, J., Nair, A., 2022. Adapting supply chain operations in anticipation of and during the COVID-19 pandemic. Omega 110, 102635.
Saad-Roy, C.M., Wingreen, N.S., Levin, S.A., Grenfell, B.T., 2020. Dynamics in a simple evolutionary-epidemiological model for the evolution of an initial asymptomatic infection stage. Proc. Natl. Acad. Sci. 117 (21), 11541–11550.
Salarpour, M., Nagurney, A., 2021. A multicountry, multicommodity stochastic game theory network model of competition for medical supplies inspired by the Covid-19 pandemic. Int. J. Prod. Econ. 236, 108074.
Sawik, T., 2022. Stochastic optimization of supply chain resilience under ripple effect: A COVID-19 pandemic related study. Omega 109, 102596.
Scarpin, M.R.S., Scarpin, J.E., Krespi Musial, N.T., Nakamura, W.T., 2022. The implications of COVID-19: Bullwhip and ripple effects in global supply chains. Int. J. Prod. Econ. 251, 108523.
Sélley, F., Besenyei, Á., Kiss, I.Z., Simon, P.L., 2015. Dynamic control of modern, network-based epidemic models. SIAM J. Appl. Dyn. Syst. 14 (1), 168–187.
Shen, Z.M., Sun, Y., 2023. Strengthening supply chain resilience during COVID-19: A case study of jd.com. J. Oper. Manage. 69 (3), 359–383.
Wong, A.S.Y., Kohler, J.C., 2020/09/25. Social capital and public health: responding to the COVID-19 pandemic. Glob. Heal. 16 (1), 88.
Wu, J., Liang, B.-Y., Fang, Y.-H., Wang, H., Yang, X.-L., Shen, S., Chen, L.-K., Li, S.-M., Lu, S.-H., Xiang, T.-D., Liu, J., Le-Trilling, V.T.K., Lu, M.-J., Yang, D.-L., Deng, F., Dittmer, U., Trilling, M., Zheng, X., 2021. Occurrence of COVID-19 symptoms during SARS-CoV-2 infection defines waning of humoral immunity. Front. Immunol. 12.
Xu, Z., Wu, B., Topcu, U., 2021. Control strategies for COVID-19 epidemic with vaccination, shield immunity and quarantine: A metric temporal logic approach. PLOS ONE 16 (3), 1–20.

Yang, W., 2021. Modeling COVID-19 pandemic with hierarchical quarantine and time delay. Dyn. Games Appl. 11, 892–914. http://dx.doi.org/10.1007/s13235-021-00382-3.

Yang, L.-X., Draief, M., Yang, X., 2017. Heterogeneous virus propagation in networks: a theoretical study. Math. Methods Appl. Sci. 40, 1396–1413.

Youssef, M., Scoglio, C., 2011. An individual-based approach to SIR epidemics in contact networks. J. Theoret. Biol. 283 (1), 136–144.

Yu, K.D.S., Aviso, K.B., 2020. Modelling the economic impact and ripple effects of disease outbreaks. Process. Integr. Optim. Sustain. 1–4.

Yuan, S., 2022. Zero COVID in China: what next? Lancet 1856–1857.

Zahiri, B., Jula, P., Tavakkoli-Moghaddam, R., 2018. Design of a pharmaceutical supply chain network under uncertainty considering perishability and substitutability of products. Inform. Sci. 423, 257–283.